

MINIATURISED RFID ANTENNAS

CHENG KOK SUEN

**A project report submitted in partial fulfilment of the
requirements for the award of Bachelor of Science
(Hons.) Physics**

**Faculty of Engineering and Science
Universiti Tunku Abdul Rahman**

August 2016

DECLARATION

I hereby declare that this project report is based on my original work except for citations and quotations which have been duly acknowledged. I also declare that it has not been previously and concurrently submitted for any other degree or award at UTAR or other institutions.

Signature : _____

Name : CHENG KOK SUEN

ID No. : 13UEB08103

Date : 30 AUGUST 2016

APPROVAL FOR SUBMISSION

I certify that this project report entitled “**MINIATURISED RFID ANTENNAS**” was prepared by **CHENG KOK SUEN** has met the required standard for submission in partial fulfilment of the requirements for the award of Bachelor of Science (Hons.) Physics at Universiti Tunku Abdul Rahman.

Approved by,

Signature : _____

Supervisor : DR LIM ENG HOCK

Date : 30 AUGUST 2016

The copyright of this report belongs to the author under the terms of the copyright Act 1987 as qualified by Intellectual Property Policy of Universiti Tunku Abdul Rahman. Due acknowledgement shall always be made of the use of any material contained in, or derived from, this report.

© 2016, Cheng Kok Suen. All right reserved.

Specially dedicated to
my beloved family and friends

ACKNOWLEDGEMENTS

I would like to thank everyone who had contributed to the successful completion of this project. I would like to express my gratitude to my research supervisor, Dr. Lim Eng Hock for his invaluable advice, guidance and his enormous patience throughout the final year project in University Tunku Abdul Rahman.

Besides that, I would like to thank my friends and seniors, especially Tan Kim Han, Tan Yan Ni and Moh Cai Wei who had given me valuable advice and insight in this project. They were always available when I needed guidance and the information obtained from them was very useful for this project.

In addition, I would also like to express my gratitude to my loving family for the motivation given to me throughout this whole project.

MINIATURISED RFID ANTENNAS

ABSTRACT

A UHF RFID reader antenna fed by the modified L-shaped probe has been proposed. The modified probe consists of an extra bend at the end of a conventional L-shaped probe. The proposed single-element antenna is able to achieve a large impedance bandwidth (760 MHz – 990 MHz), good matching (~ -30 dB) and broad CP operation (890 MHz – 940 MHz). Besides that, the antenna can achieve a maximum read range of 6.3 m in open space. A detailed parametric analysis is done to investigate the effects of some of the important design parameters on the reflection coefficient and the axial ratio. Reasonable agreement is found between the simulation model and the measured results.

The second part of this project consists the designing and fabricating of a simple Wilkinson power divider design. It is a 1-to-4 power divider. Due to the limitation of equipment, there are some extra losses in the power divider such that the actual power received is only about 20 % instead of the maximum 25 %. The measured reflection coefficients are found to be better than the simulated ones.

Lastly, the Wilkinson power divider is combined with 4 antennas to form a 2×2 array. The array is able to achieve an impedance bandwidth of 10.5 % (900 MHz – 1000 MHz), a reasonable matching level of -21 dB, and a CP bandwidth of 910 MHz - 960 MHz (5.4 %). The maximum read range is 10.8 m. Even though the proposed array is not able to operate universally in the entire UHF range, it can be used as a UHF RFID reader antenna in certain countries like Malaysia.

TABLE OF CONTENTS

DECLARATION

iii

APPROVAL FOR SUBMISSION

iv

ACKNOWLEDGEMENTS

vii

ABSTRACT

viii

TABLE OF CONTENTS

ix

LIST OF TABLES

xii

LIST OF FIGURES

xiii

LIST OF SYMBOLS / ABBREVIATIONS

xv

CHAPTER

1	INTRODUCTION	1
	1.1 Background	1
	1.2 Antenna Parameters	2
	1.2.1 S-parameter and Bandwidth	2
	1.2.2 Gain	3
	1.2.3 Polarisation	3
	1.3 Objectives and Motivation	5
	1.4 Thesis Organisation	6

2	LITERATURE REVIEW	7
2.1	Review of Methods to Achieve Broadband Operation	7
2.2	Review on Methods of Generating Circular Polarisation	8
2.3	Review on L-probe-fed UHF Reader Antennas	9
3	DESIGN METHODOLOGY	10
3.1	Introduction	10
3.2	Single Patch	10
3.3	Wilkinson Power Divider	12
3.4	2×2 Array	12
4	A BROADBAND CIRCULARLY POLARISED MODIFIED L-SHAPED PROBE ANTENNA	13
4.1	Configuration of the Single-element Antenna	13
4.2	Reflection Coefficient	15
4.3	Radiation Patterns and Read Range	16
4.4	Axial Ratio	19
4.5	Parametric Analysis	20
4.5.1	Length of the Patch, l	20
4.5.2	Width of the Patch, w	22
4.5.3	Height of the Patch, H	24
4.5.4	Vertical Length of the Probe, L_h	26
4.5.5	Horizontal Length of the Probe, L_p	27
4.5.6	Bending Length of the Probe, L_w	29
5	A STUDY ON WILKINSON POWER DIVIDER	32
5.1	Configuration of the Wilkinson Power Divider	32
5.2	Reflection Coefficient	35
5.3	Insertion Loss	39
6	A WIDEBAND CIRCULARLY POLARISED 2×2 ARRAY USING MODIFIED L-SHAPED PROBE	43

6.1	Array Configuration	43
6.2	Reflection Coefficient	45
6.3	Radiation Patterns and Read Range	46
6.4	Axial Ratio	48
7	CONCLUSION AND RECOMMENDATIONS	49
	REFERENCES	50

LIST OF TABLES

TABLE	TITLE	PAGE
4.1	Description of the Parameters Used with their Optimised Value.	15
5.1	Parameters for the Wilkinson Power Divider along with their Optimised Values.	33

LIST OF FIGURES

FIGURE	TITLE	PAGE
1.1	Time-Varying Behaviour of the Electric Field Vector for (a) Linearly Polarisation and (b) Circular Polarisation.	4
1.2	Physical Representation major axis OA and minor axis OB.	5
4.1	Geometry of the Antenna.	14
4.2	(a) Top View and (b) Side View of the Fabricated Single-element Antenna.	14
4.3	Simulated and Measured Reflection Coefficient of the Single-element Antenna.	16
4.4	Experimental Setup to Measure the Read Range.	17
4.5	Simulated Gain and the Read Range at 920 MHz in the (a) x - z plane and (b) y - z plane of the Single-element Antenna.	18
4.6	R&S®HE300CE Active Directional Antenna.	19
4.7	Simulated and Measured Axial Ratio of the Single-element Antenna.	20
4.8	Effects of the Length of the Patch, l on the (a) Reflection Coefficient and (b) Axial Ratio.	22
4.9	Effects of the Width of the Patch, w on the (a) Reflection Coefficient and (b) Axial Ratio.	24
4.10	Effects of the Height of the Patch, H on the (a) Reflection Coefficient and (b) Axial Ratio.	25

4.11	Effects of the Vertical Length of the Probe, L_h on the (a) Reflection Coefficient and (b) Axial Ratio.	27
4.12	Effects of the Horizontal Length of the Probe, L_p on the (a) Reflection Coefficient and (b) Axial Ratio.	29
4.13	Effects of the Bend Length of the Probe, L_w on the (a) Reflection Coefficient and (b) Axial Ratio.	31
5.1	Configuration of the Wilkinson Power Divider.	34
5.2	(a) Top View and (b) Back View of the Fabricated Wilkinson Power Divider.	34
5.3	Simulated and Measured S_{11} Parameter of the Wilkinson Power Divider.	35
5.4	Simulated and Measured Results for (a) S_{22}, (b) S_{33}, (c) S_{44} and (d) S_{55} for the Wilkinson Power Divider.	38
5.5	Simulated and Measured Result for (a) S_{21}, (b) S_{31}, (c) S_{41} and (d) S_{51} of the Wilkinson Power Divider.	42
6.1	Configuration of the 2×2 Array.	44
6.2	(a) Top View and (b) Side View of the Fabricated Array.	44
6.3	Simulated and Measured Reflection Coefficient of the Array.	45
6.4	Simulated Gain and the Measured Read Range in the (a) x-z plane and (b) y-z plane at 920 MHz.	47
6.5	Simulated and Measured Axial Ratio of the 2×2 Array.	48

LIST OF SYMBOLS / ABBREVIATIONS

S	S-parameter
V_-	reflected voltage, V
V_+	incident voltage, V
OA	major axis, Vm^{-1}
OB	minor axis, Vm^{-1}
Δw_y	resonance edge extension of the patch, cm
ϵ_{re}	effective dielectric constant
W	width of the patch, cm
H	height between the ground plane and the patch, cm
ϵ_r	relative dielectric constant of the substrate
f_r	resonant frequency, Hz
L	length of the patch, cm
G_x	length of the ground plane, cm
G_y	width of the ground plane, cm
s	horizontal distance between the probe and the centre, cm
k	vertical distance between the probe and the centre, cm
L_p	length of the probe, cm
L_h	height of the probe
L_w	bend length of the probe
r_1	radius of the probe
Z_o	characteristic impedance of the strip line, Ω
w	width of the strip line, cm
H_{sub}	height of the substrate, cm
l_{50_1}	length of the first 50 Ω strip line
l_{50_2}	length of the second 50 Ω strip line
l_{50_3}	length of the third 50 Ω strip line

$l_{70.71}$	length of the 70.71 Ω strip line
RFID	radio-frequency identification
EM	electromagnetic
UHF	ultra-high frequency
IEC	International Electrotechnical Commission
LP	linear polarisation
CP	circular polarisation
AR	axial ratio

CHAPTER 1

INTRODUCTION

1.1 Background

Radio-frequency identification (RFID) is a type of emerging technology that uses electromagnetic (EM) waves to identify and read tags that are attached to a certain object or place. A RFID system can be generally split into two parts, namely the tag and the reader. The tags contain electronically stored information and are able to transmit the information out to the reader. On the reader end, it picks up the transmitted signal from the tags and passes the signal into a decoder which displays the information encoded in the tags. This technology has the potential of replacing the currently used barcode system as RFID has the advantage of longer range and is able to read multiple tags at the same time.

The universal ultra-high frequency (UHF) band ranges from 860 MHz to 960 MHz is subjected to a lot of research as this frequency range has higher data transfer rate. It is regulated such that each country can only use RFID in a particular range within the universal UHF band. For example, for Malaysia it is from 919 MHz – 923 MHz, 902 MHz – 928 MHz for the United States, 952 MHz – 956.4 MHz for Japan and much more.

In the commercial UHF band, the reader antennas are generally working in two regions, either the near-field or the far-field region. Some of the commonly used antennas include dipole, Yagi-Uda, patch and others (Nikitin & Rao, 2010). In this

thesis, the latter region will be focused on. The patch antenna is of special interest because of its low profile. A patch antenna can be easily printed on a substrate, either planar or non-planar, thus it can be very cheap. However, one of the main disadvantages of using a patch antenna as a reader antenna is its very low bandwidth, typically around a few percent of the centre frequency (Balanis, 2005).

1.2 Antenna Parameters

For any reader antenna, there is a set of important parameters that define its working characteristics. The most important parameters include S-parameter, bandwidth, gain, and polarisation. Each of these parameters will be looked into more detail in the following parts.

1.2.1 S-parameter and Bandwidth

S-parameter is defined as the ratio of the reflected voltage over the incident voltage at a particular port when all the other ports are assumed to be matched (Pozar, 2005). Mathematically it can be represented as

$$S = \frac{V_-}{V_+} \quad (1.1)$$

where

S = S-parameter

V_- = reflected voltage, V

V_+ = incident voltage, V

Essentially what the S-parameter is describing is the reflection coefficient at a particular port and it is normally reported in the unit of dB. The lower the S-parameter, the less reflected voltage there is and hence more power can be transmitted to the radiating antenna.

The bandwidth of an antenna can be understood as the range of frequencies the antenna can work in with the desired characteristics. The bandwidth is related to the S-parameter. As a standard, the range of frequencies that is lower than -10 dB in the S-parameter curve is the bandwidth of the antenna. In the UHF RFID application, the antenna should have a minimum of -10 dB from 860 MHz to 960 MHz for worldwide usage.

1.2.2 Gain

Before examining the gain, the directivity of an antenna is first defined. The directivity is defined by the International Electrotechnical Commission (IEC) to be the maximum radiation intensity in a particular direction over the averaged radiation intensity (Balanis, 2005). In other words, the directivity is a figure of merit on how well the antenna radiates in one particular direction with relative to other directions. The directivity is high if the antenna radiates very well in one particular direction but not others. The gain, on the other hand, takes into account both the directivity and the efficiency of the antenna. The higher the gain, the farther the read range of the antenna.

1.2.3 Polarisation

The polarisation of an EM wave is understood as the time-varying behaviour of the electric field vector. Depending on the pattern traced out by the tip of the electric field, the polarisation can be categorised into three: linear polarisation (LP), circular polarisation (CP) and elliptical polarisation. Figure 1.1 shows how a linearly polarised and circularly polarised wave propagates with time. In the field of reader antenna, CP is more desirable than LP because the tag's relative position with the reader will not affect the signal strength. If the reader antenna is LP, then the signal will be strongest only when both the tag and the reader are placed in the same orientation as the polarisation. If the two of them are perpendicular to each other, then the signal will be at a minimum. However, for CP reader antenna, the tag can be placed arbitrarily any direction without affecting the signal strength received.

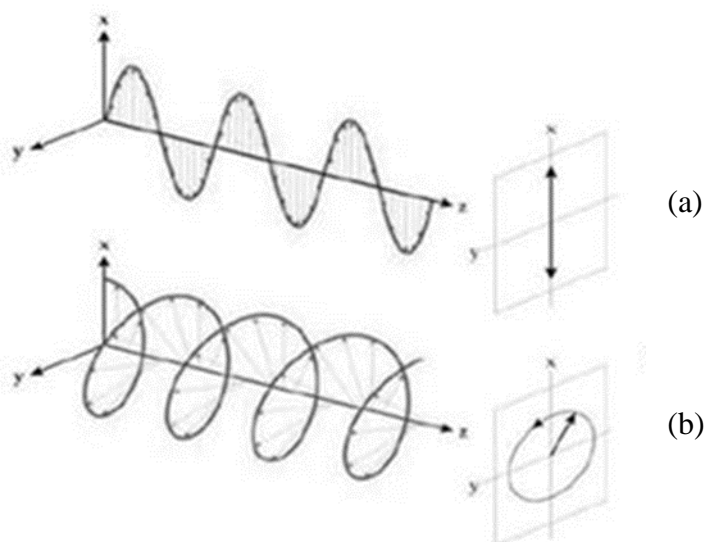


Figure 1.1: Time-Varying Behaviour of the Electric Field Vector for (a) Linearly Polarisation and (b) Circular Polarisation.

One important quantity that is able to quantify the polarisation of an antenna is the axial ratio (AR). The AR is defined as the ratio of the major axis of the electric field to the minor axis of the electric field, or mathematically

$$AR = \frac{OA}{OB} \quad (1.2)$$

where

AR = axial ratio

OA = major axis, Vm^{-1}

OB = minor axis, Vm^{-1}

The physical representation of OA and OB can be seen more clearly in Figure 1.2. The value of AR ranges from 0 dB to ∞ dB, whereby $AR = 0$ dB represents CP and $AR = \infty$ dB represents LP. For any value in between these two extremes, the antenna is having elliptical polarisation. In real life, it is almost impossible to achieve

perfect CP where the AR is equal to 0 dB. Thus, the working CP criterion is when the AR is smaller or equal to 3 dB in the desired frequency range.

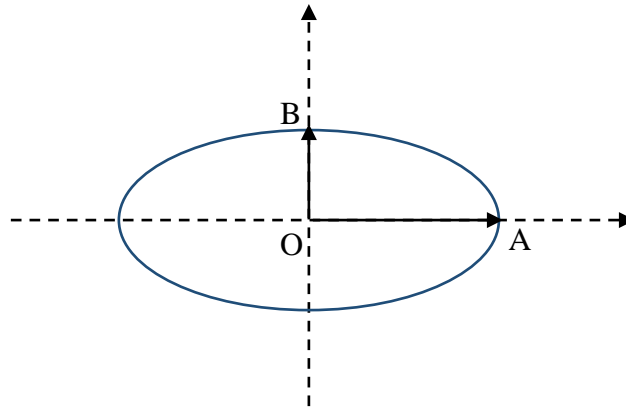


Figure 1.2: Physical Representation major axis OA and minor axis OB.

1.3 Objectives and Motivation

The main objective of this thesis is to present a novel way to generate circular polarisation using a patch antenna as a UHF reader antenna. The conventional L-probe is modified to achieve this. The UHF reader antenna is designed to have the following characteristics:

- Impedance bandwidth consisting the universal UHF frequency range
- Exhibits CP characteristics
- Gain of greater than 12 dB

In order to achieve a gain of greater than 12 dB, a 2×2 array is designed using the modified L-probe-fed patch as an unit element. For the antenna array, a Wilkinson power divider is used for splitting the input power into four channels for feeding the L-probe-fed patches.

1.4 Thesis Organisation

Chapter 1 briefly describes the background of RFID and the UHF reader antenna. The advantages and disadvantages of a patch antenna are discussed as well. Some of the basic antenna parameters are introduced. Finally, the objectives and motivation of this thesis are stated.

Chapter 2 focuses on the literature review of some methods to achieve large bandwidth and circular polarisation in the far-field reader antenna. Besides that, recent L-probe-fed UHF reader antennas are reviewed as well.

In **Chapter 3**, the design methodologies for the single-element antenna, the Wilkinson power divider and the 2×2 array antenna are discussed.

In **Chapter 4**, the details of the single-element modified L-probe-fed patch antenna are presented. The detailed geometry and parameters of the single patch and the array, along with the simulation and measurement results, are included as well. Besides that, a detail parametric analysis is done to study the effects of different parameters.

Chapter 5 gives the configuration of the Wilkinson power divider being used for the array. The simulated and measured results for all 5 ports are presented.

Chapter 6 investigates the 2×2 array which is designed by combining the unit element in Chapter 2 with the Wilkinson power divider in Chapter 4. Similar as above, the simulated and measured results of the proposed array are presented and studied.

At last, **Chapter 7** gives a conclusion to this project and some recommendations for future works.

CHAPTER 2

LITERATURE REVIEW

2.1 Review of Methods to Achieve Broadband Operation

As mentioned above, one of the main disadvantages of using a patch antenna is its very small bandwidth. In order to overcome this, in 1998, Mak et al. proposed a new feeding method which is the L-shaped probe. The probe looks like a horizontal 'L' and they had shown that the bandwidth can be as high as 35 %. In order to implement this feeding method, the substrate used is air substrate. The original literature had shown for the frequency range from 3 GHz to 6 GHz. However, the reported antenna design was linearly polarised.

Another method to achieve broadband operation is to use the probe-fed meandered strip technique (Wang et al., 2010). First, both the radiating patch and the meandered strip are printed on two separate FR4 substrates, with the radiating patch elevated with some distance above the meandered strip. Then, an SMA connector is connected to the strip and a second probe is connected from the strip to the radiating patch. They have shown that this method of feeding is able to operate in the band of 865 MHz – 928 MHz. Although this is slightly smaller than the universal UHF range, this method is simple and low-cost.

Lastly, one of the common ways to get large bandwidth is to use stacked elements. In general, the antenna design consists of not only a single radiating patch but also another parasitic patch placed above or below the radiating patch. Some

examples include Boo et al. (2009) who used two rectangular patches in their design and Liu, Liu and Tentzeris (2015) proposed using 2 coin-shaped (a circle with a square slot in the middle) patches. Similar to the aforementioned methods, the operating bandwidth is in the universal UHF range (Sun and Lee, 2008).

2.2 Review on Methods of Generating Circular Polarisation

Circular polarisation in the patch resonator can be achieved through the principle of detuning degenerate modes (Garg, 2001). The electric field radiated can be resolved into 2 orthogonal degenerate modes denoted by 1 and 2. With suitable perturbation or modification, the two modes will have the same amplitude but one is 90° out of phase with respect to the other one. This is the requirement of CP and thus, CP is achieved.

One of the most common methods used to implement CP in UHF reader antenna is to truncate a patch. For a rectangular patch, the edges diagonal to each other is sliced off in this method, forming a hexagonal patch (Wang et al., 2010; Wang et al., 2011; Tang, Zhan and Liu, 2012). The two truncated edges provide the necessary perturbation to generate the two degenerate modes for CP. CP has also been generated by using truncated triangular patch. Sim and Hsu (2013) proposed an equilateral triangular patch with a semi-circular notch at each of its sides. On the other hand, Yeh et al. (2015) used a right-angle triangular patch with a slit in addition to a semi-circular parasitic patch.

Besides that, CP can be generated by changing the probe's position or using multiple probes. One good example of using a single probe to achieve CP is given by Boo et al. (2009). Their design consists of a simple non-truncated rectangular patch with the probe placed along the diagonal line connecting two corners. When using multiple probes, the waves must be excited to be 90° out-of-phase relative to different probes. Two probes can be placed at a physical length of equal to quarter-

wavelength in order to meet the criteria of 90° phase difference for CP (Liu, Liu and Tentzeris, 2015)

2.3 Review on L-probe-fed UHF Reader Antennas

After the demonstration of L-shaped probe by Mak et al., many researchers have successfully deployed the L-shaped probe for designing various CP antennas for the UHF RFID purposes. Xu, Chen and Qing (2012) had reported an arc-shaped L probe to feed a suspended circular patch with multiple slots to achieve a CP bandwidth covering 800 MHz - 1000 MHz. Although this design has large bandwidth, involvement of multiple slots may complicate the fabrication process.

An L-shaped probe was deployed for exciting two slot-loaded circular patches as well (Chen and Sim, 2014). In this case, the two patches are stacked for achieving a CP bandwidth of 14.2%. The only shortcoming here is that it requires the use of double-layer structure, which may increase the manufacturing costs.

Radiating patches in other shapes are also incorporated with the L probe for designing CP reader antennas. A single-layered triangular patch with a notch (Sim and Hsu, 2013) and a combination of the triangular and semicircular patches (Yeh et al., 2015) are proposed for generating CP operation. The impedance bandwidths of the two designs are 25.4 % and 19.9 %, respectively, and the corresponding CP bandwidths are about 3.0 % and 4.3 %.

CHAPTER 3

DESIGN METHODOLOGY

3.1 Introduction

The whole design of this project consists of four parts: 1) the single patch, 2) the Wilkinson power divider and 3) combined 2×2 array with the Wilkinson power divider. The simulation and optimisation of each part are all done using the commercial software CST Microwave Studio.

3.2 Single Patch

Since this design is a modified version of an L-shaped probe-fed patch antenna, the physical dimensions of this design are first roughly determined by the formulation given by Mak et al. (2000). The height measure between the ground plane and the probe H and the width of the radiating patch W is first set to be some value. Next, the resonance edge extension of the patch is given by

$$\Delta w_y = 0.412 \frac{(\varepsilon_{re} + 0.3) \left(\frac{W}{H} + 0.264 \right)}{(\varepsilon_{re} + 0.258) \left(\frac{W}{H} + 0.813 \right)} H \quad (3.1)$$

where

Δw_y = resonance edge extension of the patch, cm

ε_{re} = effective dielectric constant

W = width of the patch, cm

H = height between the ground plane and the patch, cm

The effective dielectric constant is defined as

$$\epsilon_{re} = \frac{\epsilon_r + 1}{2} + \frac{\epsilon_r - 1}{2} \left(1 + \frac{10H}{W} \right)^{-\frac{1}{2}} \quad (3.2)$$

where

ϵ_r = relative dielectric constant of the substrate

From equation (3.1) and equation (3.2), the length of the patch can be calculated with the resonant frequency of 920 MHz using

$$f_r = \frac{c}{2(L + 2\Delta w_y)\sqrt{\epsilon_{re}}} \quad (3.3)$$

where

f_r = resonant frequency, Hz

L = length of the patch, cm

Using the rough estimated physical dimensions of the patch, along with other parameters relating to the modified probe, the design is drawn into CST and simulated. The antenna is optimised by varying the parameters until the working frequency is in the UHF range and also has CP. The details of all the parameters used will be explained with much more clarity in Chapter 3.

3.3 Wilkinson Power Divider

The Wilkinson power divider is a type of power divider that is able to have all the ports matched in addition to having isolation between the outputs (Pozar, 2005). Since the design cannot have four feeding ports, a 1-to-4 Wilkinson power divider is needed so that one port is able to feed all 4 patches simultaneously with higher efficiency. In essential, the Wilkinson power divider acts as a way to split the input power equally and in phase to each of the 4 patches, so each patch will receive 1/4 of the input power and will not interfere with each other.

The Wilkinson power divider used for this design is a 1-to-2 divider, then only following by a 2-to-4 divider, so it is a two-step Wilkinson power divider. This design will have higher loss, but it is easier to fabricate.

The design overview of the Wilkinson power divider is as follows: first, a 50 Ω port is fed to a 50 Ω strip line. Then the 50 Ω line is connected to two 70.71 Ω strip lines which act as quarter-wave impedance transformer. Then each of the 70.71 Ω strip lines is connected to another 50 Ω line. Next, the first part of the design is repeated on the second 50 Ω line to produce a 1-to-4 divider. The whole divider is then simulated again in CST to double check the design.

3.4 2×2 Array

Lastly, the 2×2 array is combined together with the Wilkinson power divider and is simulated in CST. Further optimisation is carried out to tune the antenna to the best working characteristics.

CHAPTER 4

A BROADBAND CIRCULARLY POLARISED MODIFIED L-SHAPED PROBE ANTENNA

4.1 Configuration of the Single-element Antenna

The single patch antenna consists of three elements: the copper ground plane, the modified L-shaped probe, and the radiating patch. The radiating patch is at a certain height above the ground plane, using foam as a support. Both the ground plane and the radiating patch are made up of rectangular aluminium plates.

As for the probe, it is essentially a common L-shaped probe with an extra bend at the end of the probe at an angle of 90° . So, the new modified L-shaped probe now has three sections and each side is orthogonal to each other. The probe is made up of a copper wire inserted into a hollow SMA connector, which is then bolted to the ground plane. The probe is placed with an offset along the line joining the two opposite vertices as shown in Figure 4.1 and Figure 4.2(b).

Figure 4.1 shows the design of the reader antenna with all the parameters labelled. On the other hand, Table 4.1 lists out all of the parameters used in this design, along with their descriptions and the optimised value for each parameter.

The simulated and measured results for the S-parameter, gain, radiation pattern, axial ratio and the measured read range are discussed in the following sections.

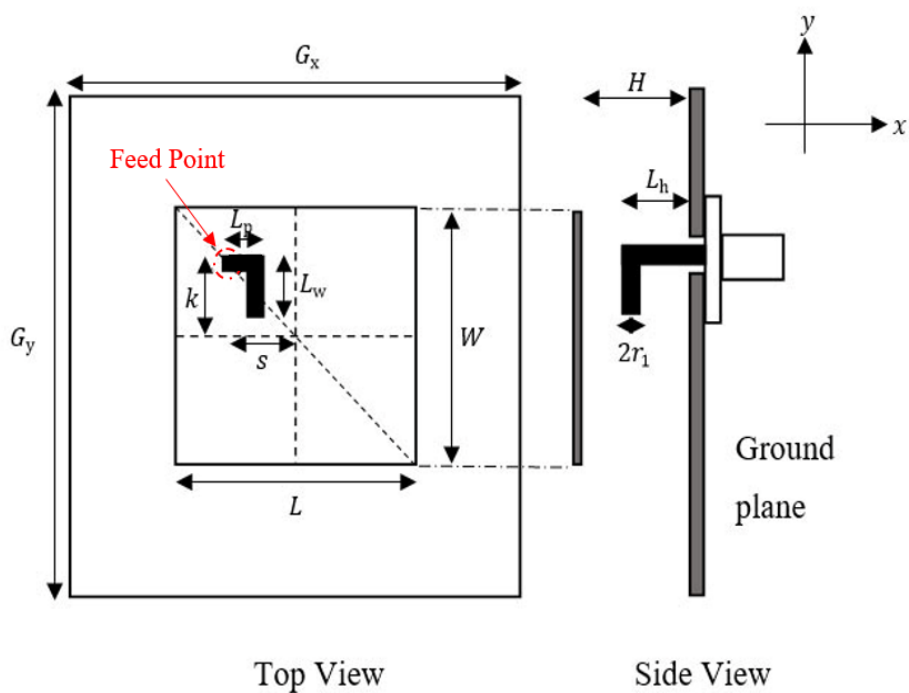


Figure 4.1: Geometry of the Antenna.

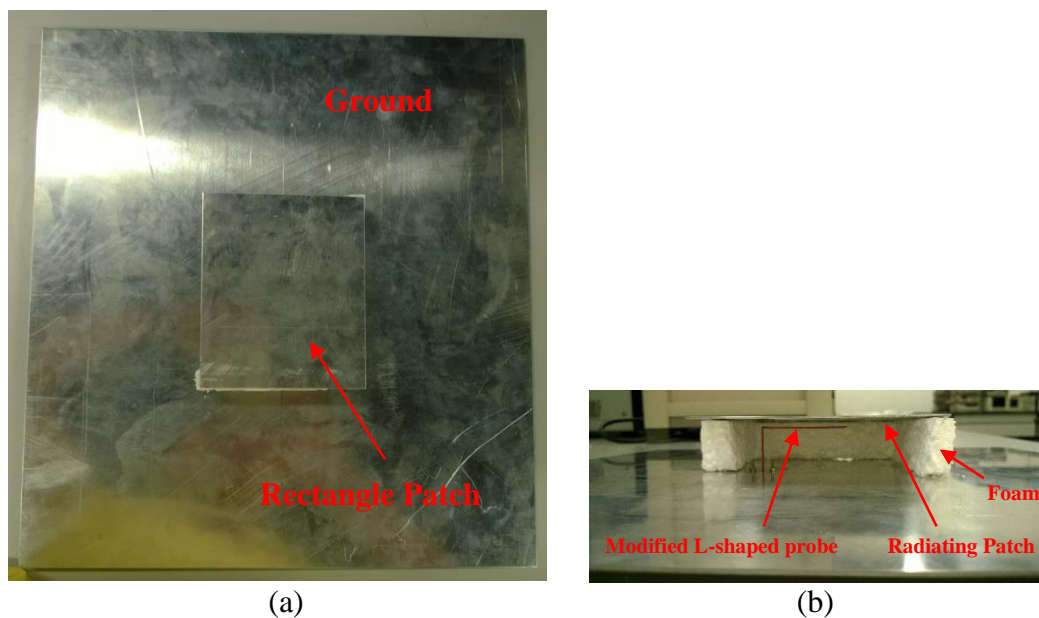


Figure 4.2: (a) Top View and (b) Side View of the Fabricated Single-element Antenna.

Table 4.1: Description of the Parameters Used with their Optimised Value.

Symbol of Parameter	Description	Optimised Value/cm
G_x	Length of the ground plane	35.5
G_y	Width of the ground plane	40.5
L	Length of the patch	11
W	Width of the patch	13.9
H	Height between the ground plane and the patch	3
s	Horizontal distance between the probe and the centre	2.75
k	Vertical distance between the probe and the centre	3.475
L_p	Vertical Length of the probe	0.5
L_h	Horizontal Length of the probe	2.5
L_w	Bend length of the probe	5
r_1	Radius of the probe	0.05

4.2 Reflection Coefficient

The R&S® ZVB8 Vector Network Analyzer (VNA) is used to measure the S-parameter or the S_{11} of the proposed antenna. As seen from Figure 4.3, the measured result is in good agreement with the simulated result. The two resonances of the prototype are seen to be at 800 MHz and 880 MHz, respectively. As compared to the simulated result, the first resonance is in good agreement while the second resonance is slightly lower than the simulated 905 MHz. In terms of magnitude, the measured result shows a better matching as the magnitude of the two dips are -25 dB and -29 dB respectively. However, for the impedance bandwidth, the measured result is smaller than the simulated one such that the prototype can only achieve a bandwidth of 26.3 % (760 MHz to 990 MHz). The simulated bandwidth is from 760 MHz to 1050 MHz, which corresponds to 32.0 %.

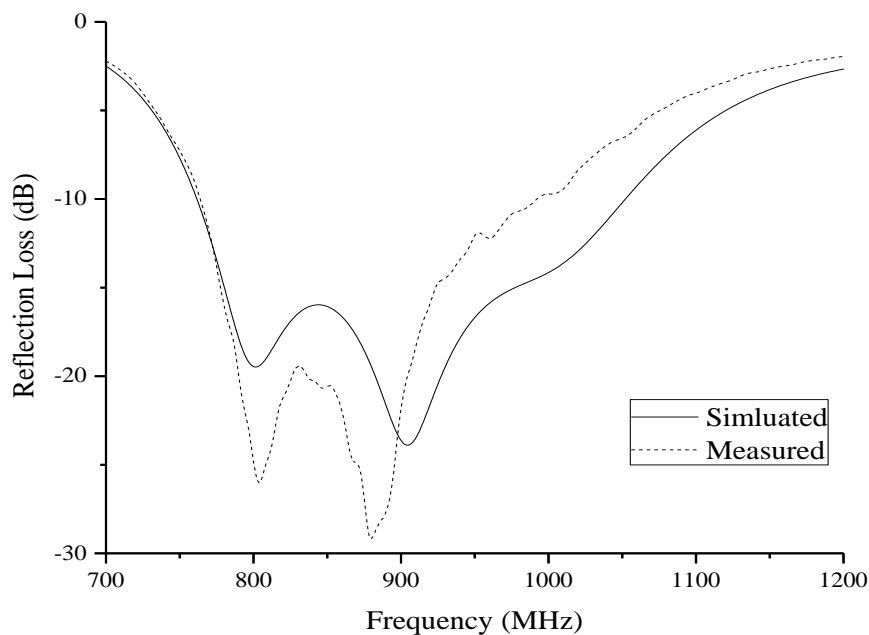


Figure 4.3: Simulated and Measured Reflection Coefficient of the Single-element Antenna.

4.3 Radiation Patterns and Read Range

Since the proposed antenna is CP, so in order to measure the radiation pattern in terms of its gain, one would need another CP antenna as well. Due to the lack of a CP antenna, the radiation pattern is instead measured in terms of the read range of the antenna using a commercially available RFID tag. First of all, the prototype is mounted on a turntable where the angle between the antenna and the tag can be varied. The antenna is then connected to a Mi-1801B reader unit, which is in turn connected to a laptop to transfer the data. The power of the reader is set to be 30 dBm. As for the tag, it is stuck on a piece of foam supported by a stand. The stand is adjusted such that the tag is always level with the centre of the antenna. A string is used to ensure the tag is always aligned with respect to the antenna. The tag used in this measurement is an RAPITA® UHF RFID tag. The experimental setup is shown in Figure 4.4.

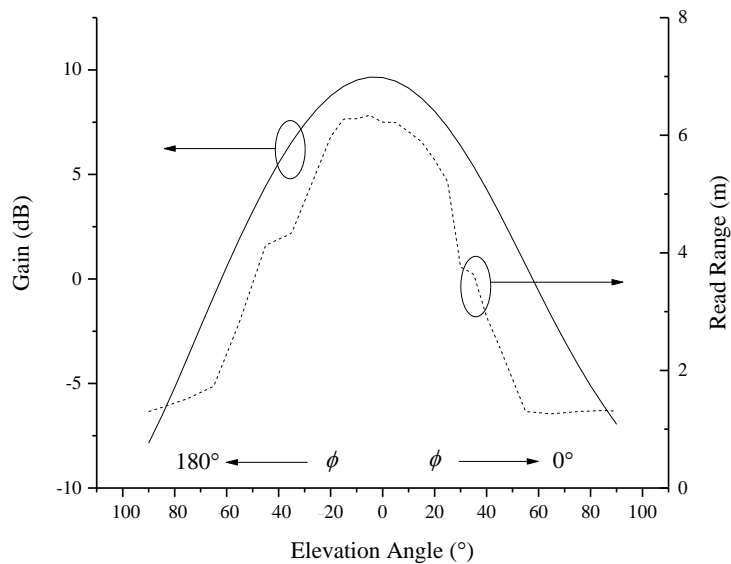


Figure 4.4: Experimental Setup to Measure the Read Range.

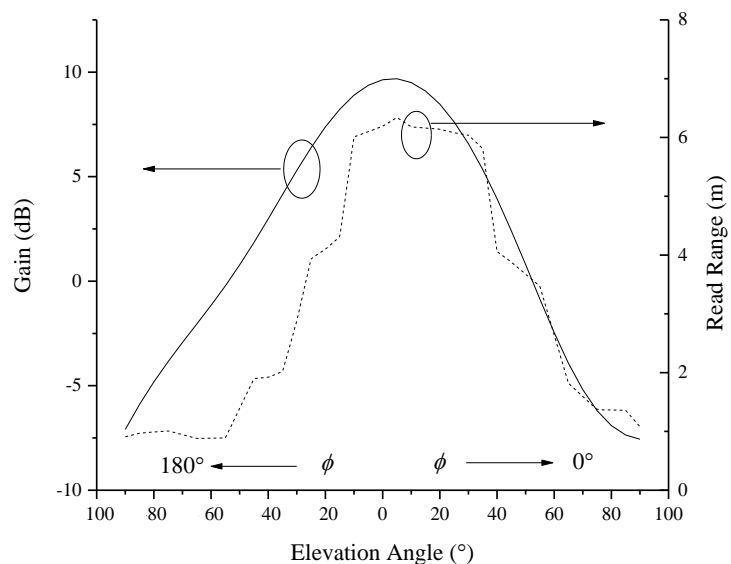
Figure 4.5(a) and (b) show the simulated gain and the measured read range of the single-element antenna at 920 MHz in the x - z plane and y - z plane respectively. In the x - z plane, the gain is at a maximum of 9.7 dB occurs at 5° ($\phi \rightarrow 180^\circ$) and the gain decreases as the elevation angle between the tag and the antenna increases. The minimum gain happens at 90° whereby the gains at these two angles are only -6.92 dB and -7.81 dB respectively. This trend is reflected in the measurement of the read range. The maximum read range is 6.3 m and the read range decreases with increasing angle. At the two extremes, the measured read range is only about 1.3 m.

As for the y - z plane, the general pattern is the same whereby both the gain and the read range decrease-as the angle increases. However, for this plane, there is a difference in the angle where the maximum gain is located. The peak gain and the maximum read range for this plane is the same as the x - z plane at 9.7 dB and 6.3 m respectively, but the angle where it occurs is now changed to 5° ($\phi \rightarrow 0^\circ$). Another interesting characteristic in this plane is that the read range in the $\phi \rightarrow 0^\circ$ direction is larger than that of in the $\phi \rightarrow 180^\circ$ direction. As seen from Figure 4.5(a), the read range in the x - z plane is more or less symmetrical about the centre 0° . However, the read range pattern shown in Figure 4.5(b) is skewed towards the right. This is due to the higher gain in the $\phi \rightarrow 0^\circ$ direction. For example, at 40° ($\phi \rightarrow 0^\circ$), the simulated

gain is 3.94 dB while the gain at 40° ($\phi \rightarrow 180^\circ$) is only 2.97 dB. This corresponds to a difference of approximately 2 m in the read range.



(a)



(b)

Figure 4.5: Simulated Gain and the Read Range at 920 MHz in the (a) x - z plane and (b) y - z plane of the Single-element Antenna.

4.4 Axial Ratio

The axial ratio of the fabricated antenna is measured by using the rotating linear polarised antenna technique. First of all, the proposed antenna is set up as the transmitting antenna while an R&S®HE300CE Active Directional Antenna is set up as the receiving antenna. The directional antenna is shown in Figure 4.6. Next, the power received at the receiving end is measured for a frequency range of 860 MHz to 960 MHz using a spectrum analyser. Then, the receiving antenna is rotated 90° so that the electric field received is orthogonal to the configuration just now and the power is measured again. The axial ratio is then found by subtracting the two measured powers in the units of dB.



Figure 4.6: R&S®HE300CE Active Directional Antenna.

Figure 4.7 shows the simulated and measured axial ratio of the single-element patch antenna. As seen from the figure, the proposed antenna is able to achieve a CP bandwidth of 5.5 % (890 MHz - 940 MHz) and the lowest axial ratio magnitude that can be achieved is 1.6 dB at 910 MHz. When compared to the simulated result, the CP bandwidth is seen to have shifted towards the lower frequencies and the magnitude is larger than the simulated magnitude as well. From this result, the proposed antenna is not able to have CP in the whole universal UHF range, so further

work can be done to push the axial ratio magnitude to be smaller than 3 dB for the whole range.

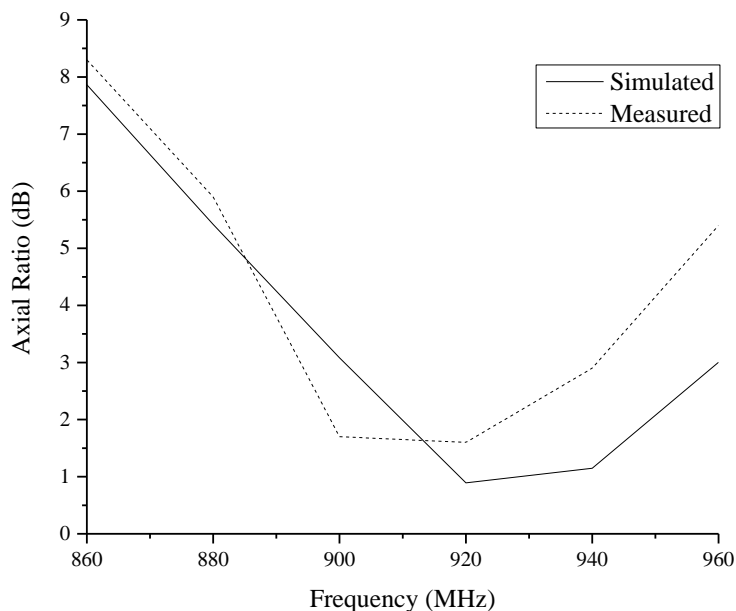


Figure 4.7: Simulated and Measured Axial Ratio of the Single-element Antenna.

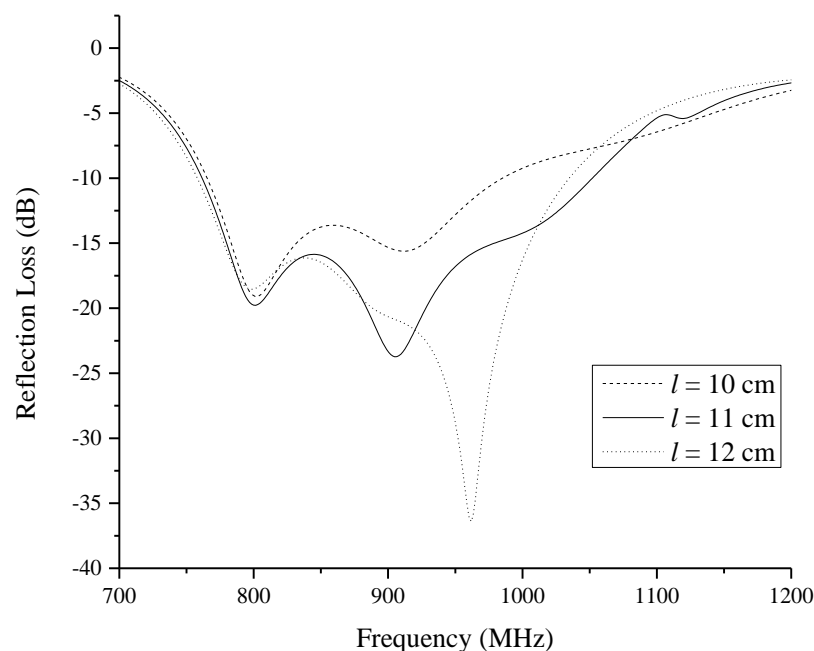
4.5 Parametric Analysis

In order to further investigate the effects of the parameters on the reflection coefficient and the axial ratio of the antenna, a comprehensive parametric analysis is performed. 6 parameters are studied, namely l , w , H , L_h , L_p , and L_w .

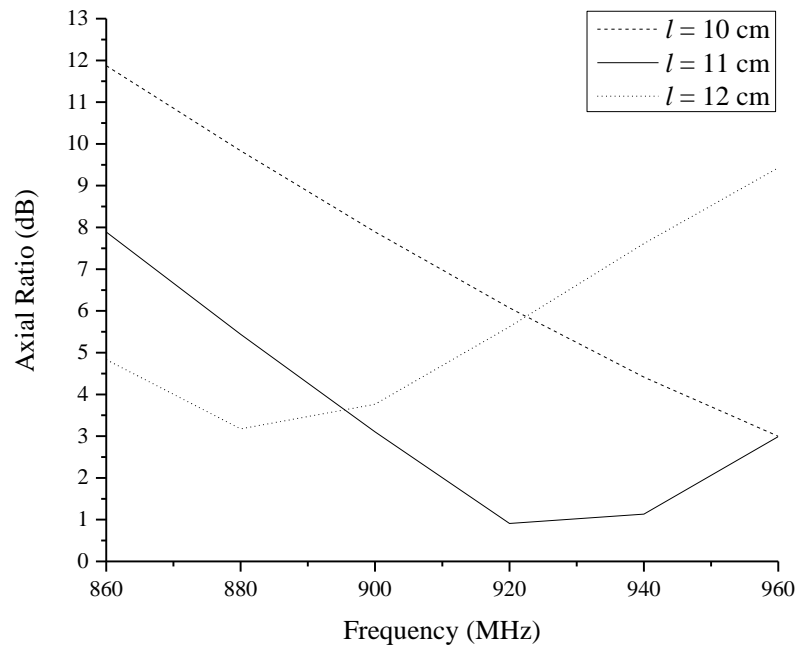
4.5.1 Length of the Patch, l

First of all, the effects of the length of the patch l are investigated. The effects of this particular parameter on the reflection coefficient and axial ratio are shown in Figure 4.8(a). For the reflection coefficient or S_{11} parameter, only the second resonant dip is seen to change when the length changes. The first dip at 800 MHz has not been affected while the second dip shifts to a higher frequency when the length of the

patch is increased. When $l = 10$ cm and 11 cm, the resonant frequency is still around 905 MHz, however when the length is increased to 12 cm, the dip occurs at 960 MHz. In terms of magnitude, the matching is becoming better when the length increases as the magnitude of the reflection loss is seen to decrease from -15 dB to -35 dB at $l = 12$ cm. With reference to Figure 4.8(b), the effect of this parameter on the axial ratio is presented. For $l = 10$ cm, there is no CP operation in the UHF region as the axial ratio is more than 3 dB for the whole frequency range. When l increases, the CP bandwidth is seen to move towards the higher frequencies region. When $l = 11$ cm, which is the proposed dimension, the CP bandwidth is from 890 MHz - 940 MHz. When $l = 12$ cm, there exists a possibility that the CP operation region lies beyond the UHF range because the axial ratio is still decreasing without a clear turning point. Since the antenna is designed for UHF RFID reader antenna purposes, this result is not desirable.



(a)



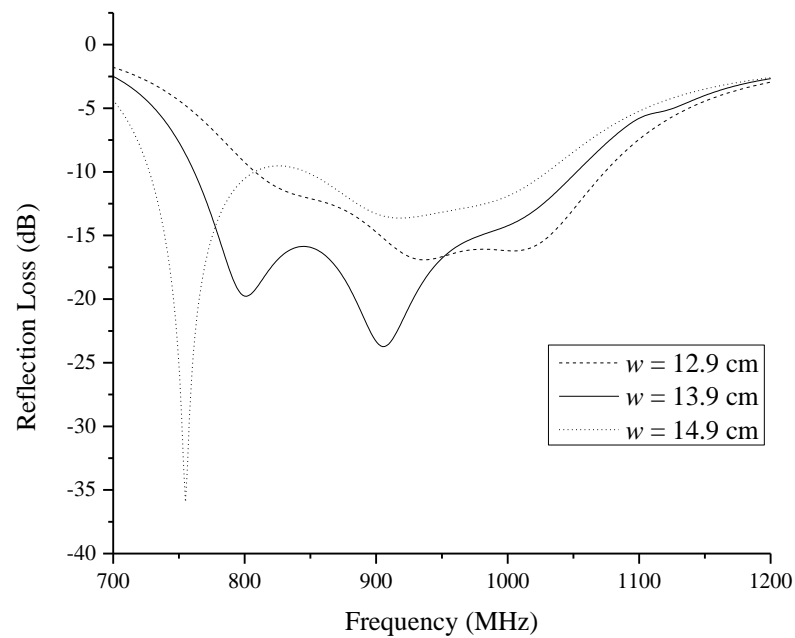
(b)

Figure 4.8: Effects of the Length of the Patch, l on the (a) Reflection Coefficient and (b) Axial Ratio.

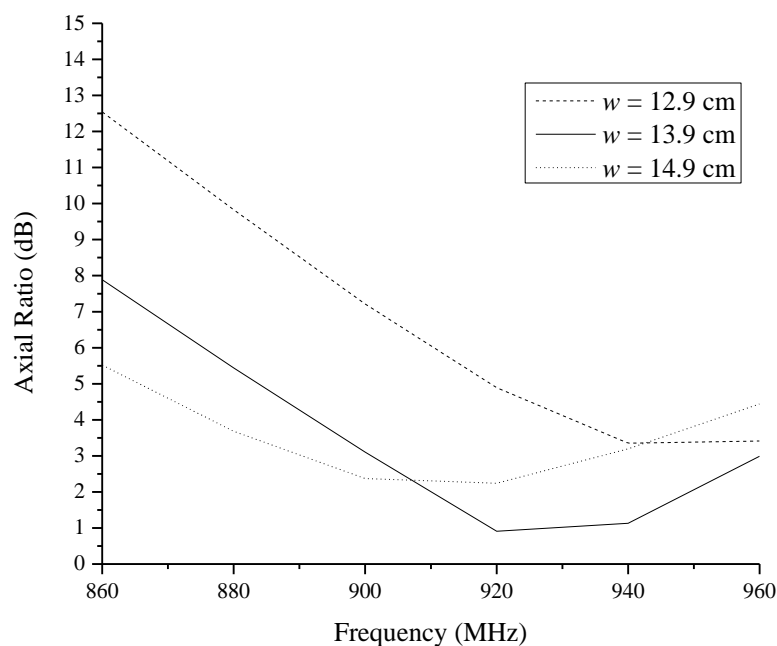
4.5.2 Width of the Patch, w

Figure 4.9(a) and (b) show the effects of the width of the patch w on the reflection coefficient and the axial ratio respectively. For this parameter, the value is varied from 12.9 cm to 14.9 cm with 1 cm increment. With reference to Figure 4.9(a), both of the resonant dips are affected by the width such that they shift towards the lower frequencies when the width increases. The bandwidth for the patch with $w = 12.9$ cm is from 800 MHz to 1050 MHz, which is still able to cover the whole universal UHF range. But magnitude wise, the matching is not as good as the proposed dimension as the lowest dip has only a magnitude of about -17 dB as oppose to the proposed -25 dB. On the other hand, when $w = 14.9$ cm, the matching of the first resonant dip becomes very good at a magnitude of -35 dB at 750 MHz. However, due to this good matching, the bandwidth is compromised. The bandwidth is reduced to 9.4 % (737

MHz - 810 MHz) only, hence it is not suitable for UHF RFID purposes. With reference to Figure 4.9(b), the axial ratio for the three values of w is shown. For $w = 12.9$ cm, there is no CP operation observed. When the width of the patch is equal to 14.9 cm, there is CP operation from 890 MHz to 935 MHz which corresponds to a CP bandwidth of 4.9 %. This is smaller than the proposed dimension of 13.9 cm which has a CP bandwidth of 5.5 %.



(a)



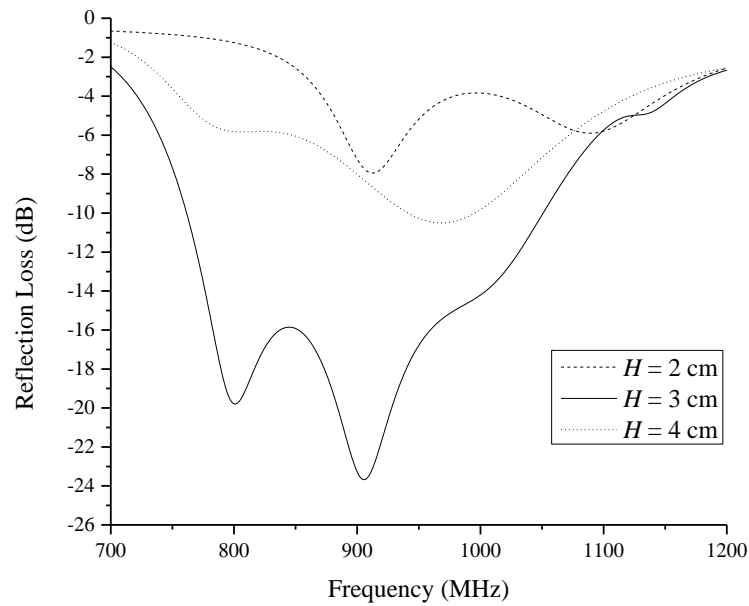
(b)

Figure 4.9: Effects of the Width of the Patch, w on the (a) Reflection Coefficient and (b) Axial Ratio.

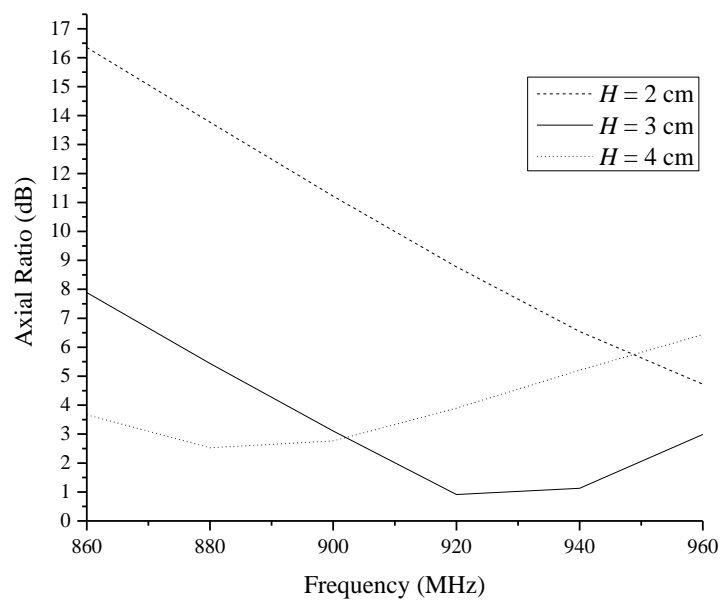
4.5.3 Height of the Patch, H

Figure 4.10(a) shows the effects of different height of the patch relative to the ground plane ($H = 2$ cm, 3 cm and 4 cm) on the reflection coefficient. As seen from the figure, the reflection coefficient is very sensitive to the height of the patch. This is because even a 1 cm difference from the proposed height ($H = 3$ cm) can totally detune the resonance of the antenna. At $H = 2$ cm and 4 cm, the two resonant dips are still visible but the matching is very bad whereby the smallest reflection is only at around -10 dB. As for the axial ratio, the effects are shown in Figure 4.10(b). The CP bandwidth is seen to shift towards the lower frequencies when H increases. For $H = 2$ cm, there is no CP operation from 860 MHz to 960 MHz as the magnitude of the axial ratio is more than 3 dB in this frequency range. For $H = 4$ cm, a small CP bandwidth is observed from 870 MHz to 905 MHz (3.9 %). If the reflection

coefficient is taken into account as well, then this configuration of the antenna is not desirable as well.



(a)

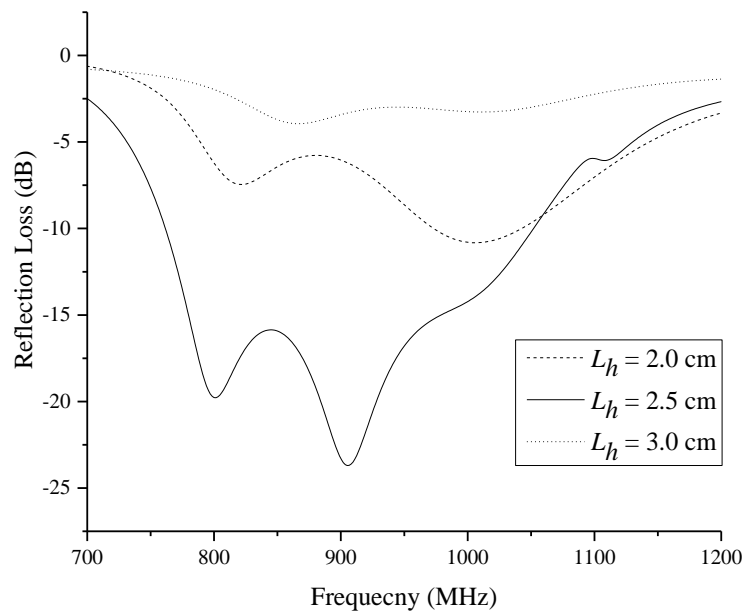


(b)

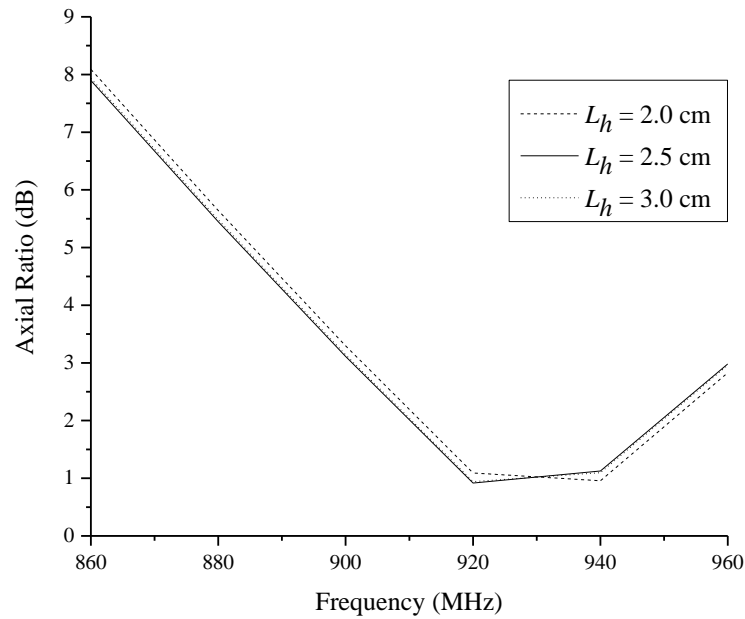
Figure 4.10: Effects of the Height of the Patch, H on the (a) Reflection Coefficient and (b) Axial Ratio.

4.5.4 Vertical Length of the Probe, L_h

Now, the parameters involving the modified L-shaped probe are studied. The first parameter to be investigated is the first section of the probe L_h . The effects on the reflection loss and axial ratio are presented in Figure 4.11(a) and (b) respectively. For the reflection coefficient, changes in L_h affect the magnitude of the reflection coefficient significantly as shown in the figure. Similar to the parameter H , a small change in L_h is able to worsen the performance of the antenna by a lot. With only a 0.5 cm difference from the proposed dimension of 2.5 cm, the matching of the antenna is very poor. For $L_h = 2.0$ cm, there is still one resonant dip at 1000 MHz that has a magnitude lower than -10 dB, but the actual magnitude is only at approximately -11 dB. While for $L_h = 3.0$ cm, the antenna cannot even be used as the matching is very bad. Figure 4.11(b) shows the effects of this parameter on the axial ratio. The first length of the probe has a significant effect on the reflection coefficient, but the same thing cannot be said about the axial ratio. From Figure 4.11(b), there is hardly any changes in the axial when the value of L_h is varied. Hence, L_h is one of the parameters used to tune the reflection coefficient without affecting the axial ratio.



(a)



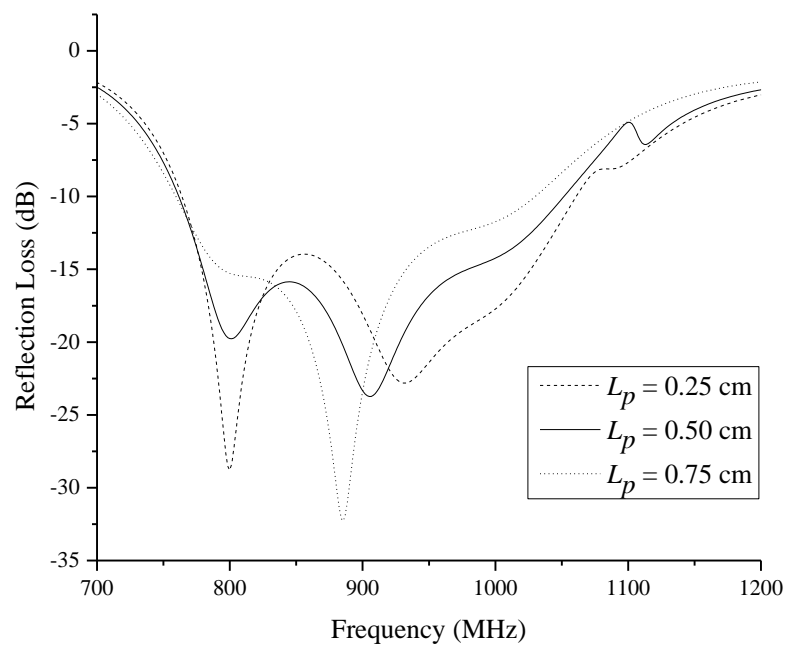
(b)

Figure 4.11: Effects of the Vertical Length of the Probe, L_h on the (a) Reflection Coefficient and (b) Axial Ratio.

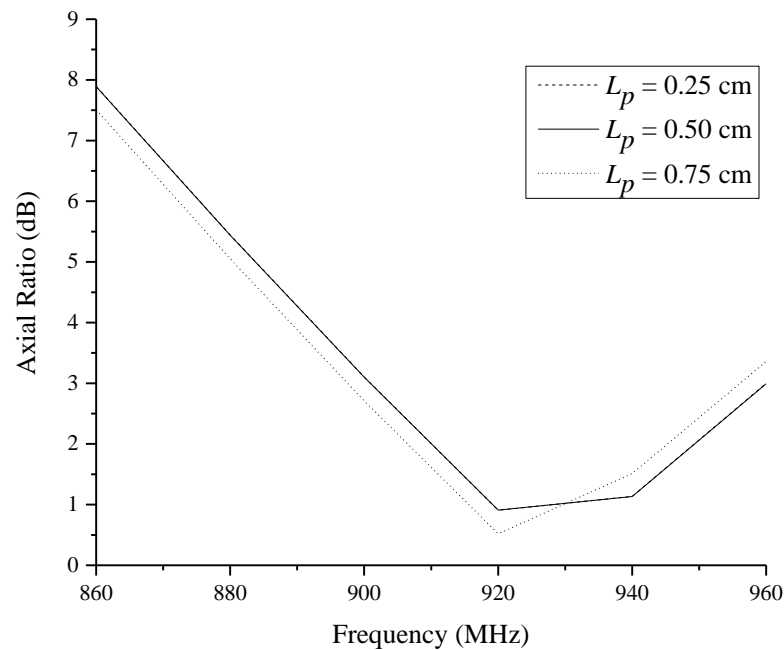
4.5.5 Horizontal Length of the Probe, L_p

Figure 4.12(a) shows the effect of the second side of the probe L_p on the reflection coefficient. From the figure, one can see that now both the resonant dips are affected by this parameter. Focusing at the first resonant dip first, one can see that the frequency of resonance for all three configurations is the same at 800 MHz, but the matching is greatly affected. Starting from $L_p = 0.25$ cm, the magnitude of the reflection coefficient is at about -30 dB, following by -20 dB for $L_p = 0.50$ cm, and lastly for $L_p = 0.75$ cm, the magnitude is -15 dB. From this trend, it can be concluded that as the value of L_p increases, the matching of the first resonant dip will get worse without affecting the resonance frequency. As for the second resonant dip, now both the resonance frequency and the magnitude are affected by changing L_p . From $L_p = 0.25$ cm to 0.75 cm, the second dip is seen to have shifted from 933 MHz to 905 MHz and lastly to 885 MHz respectively. The magnitudes on the other hand for the

three configurations are -23 dB, -24 dB and -32 dB respectively. Thus, the second resonance will shift towards the lower frequencies while the magnitude will become smaller when the value of L_p increases. In terms of bandwidth, it can be seen that the bandwidth is not affected and it is the same for all three configurations. Figure 4.12(b) shows the axial ratio for the three configurations. The only noticeable difference for this three value is that when $L_p = 0.75$ cm, a good axial ratio of 0.5 dB is achievable at 920 MHz, which is better than the proposed dimension.



(a)



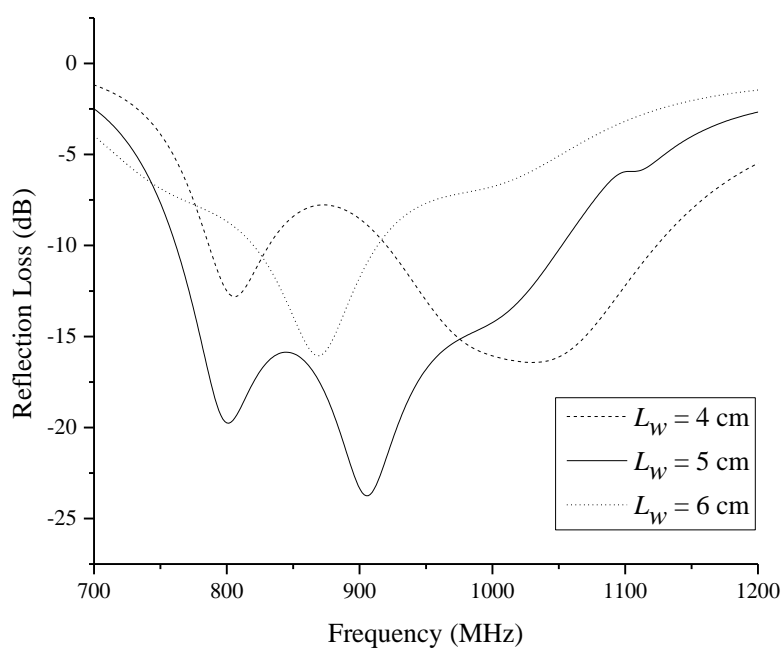
(b)

Figure 4.12: Effects of the Horizontal Length of the Probe, L_p on the (a) Reflection Coefficient and (b) Axial Ratio.

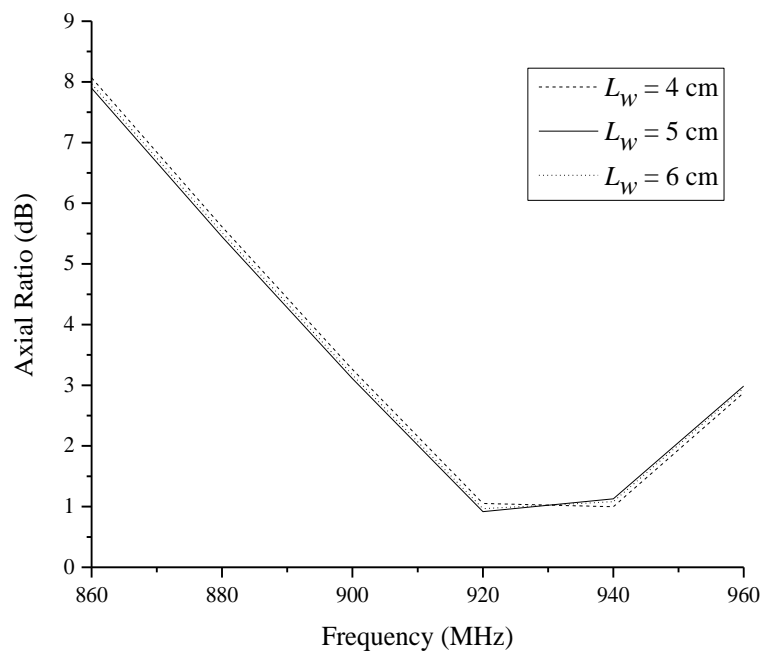
4.5.6 Bending Length of the Probe, L_w

The last parameter to be studied is the third section of the probe, L_w . Figure 4.13(a) presents the reflection coefficient of the three different values of L_w ($L_w = 4$ cm, 5 cm and 6 cm). As compared to the proposed dimension of 5 cm, the magnitude of the reflection loss of $L_w = 4$ cm is seen to be larger. The magnitudes of the two dips are about -13 dB and -17 dB respectively. Besides that, the second resonant dip is shifted towards a higher frequency of 1000 MHz. Even though the two dips are still present, but only the second dip is relevant as it covers the UHF range. A bandwidth of 19.6 % (920 MHz - 1120 MHz) is achievable for this particular value of L_w . This impedance bandwidth only covers the upper region in the UHF, so the usage of this antenna is limited to those countries that use the higher frequencies in the UHF range. One example would be Japan. When L_w is equal to 6 cm, only one resonant dip is observed at 870 MHz with a magnitude of -16 dB. The bandwidth of this value of L_w

is the smallest among the three, whereby it is only 10.4 % (820 MHz - 910 MHz). This time, the lower region of the UHF is covered only. This particular configuration of the antenna cannot be used universally around the wall, but it still has the potential to be used in those countries which are using the lower frequencies RFID, for example, Europe. The effects on the axial ratio are presented in Figure 4.13(b). From the figure, one can conclude that the axial ratio is not affected by the third length of the probe L_w .



(a)



(b)

Figure 4.13: Effects of the Bend Length of the Probe, L_w on the (a) Reflection Coefficient and (b) Axial Ratio.

CHAPTER 5

A STUDY ON WILKINSON POWER DIVIDER

5.1 Configuration of the Wilkinson Power Divider

Since a 50 Ω coaxial probe is used to feed the Wilkinson power divider, a strip line with characteristic impedance of 50 Ω is used at port 1 for matching condition. After that, the 50 Ω line is connected to two 70.71 Ω strip lines. Next, each 70.71 strip lines are connected to a second 50 Ω line and the whole process is repeated to have a four-way divider. Three 100 Ω resistors are connected between each of the ends of the 70.71 Ω lines to finish the Wilkinson power divider.

The equation to calculate the width of the strip lines is given by Bahl and Trivedi (1977) to be

$$Z_o = \frac{120\pi}{\sqrt{\epsilon_{re}} \left[\frac{w}{H_{sub}} + 1.393 + \frac{2}{3} \ln \left(\frac{w}{H_{sub}} + 1.444 \right) \right]} \quad (5.1)$$

where

Z_o = characteristic impedance of the strip lines, Ω

w = width of the strip line, cm

H_{sub} = height of the substrate, cm

while ϵ_{re} is defined in Eq. (3.2). The calculated width for the 50Ω lines, w_{50} and 70.71Ω lines, $w_{70.71}$ are 0.287 cm and 0.151 cm respectively.

Since this is a 1-to-4 power divider, 5 ports are needed. Starting at the middle 50Ω line, a normal SMA connector is soldered to the power divider at a distance of 2.4 cm from the edge of the line. This port is defined as port 1. The second port is defined at the top right corner of the 50Ω strip line. The port is placed at a distance of 0.5 cm from the edge of the line. Next, the port is defined in a counter-clockwise direction, so port 3 is defined at the top left corner. Port 3 is soldered at a distance of 1.2 cm from the edge. Similar to port 3, port 4 at the lower left corner is placed 1.2 cm from the edge of the line while for port 5, it is the same as port 2 with an offset of 0.5 cm from the edge.

The whole Wilkinson power divider is printed on a FR-4 substrate with a thickness of 1.5 mm and also a copper ground plane at the bottom. The size of the design is $55 \text{ cm} \times 55 \text{ cm}$. Since the equipment available is not able to etch an FR-4 of such size in one piece, the design is separated into several pieces and etched separately. After each piece is done, the individual parts are patched up together using copper tape. This can be seen in Figure 5.2(a) where the boundaries between each piece are quite obvious. For the ground plane, the same patching of copper tape is used so that the whole ground plane is one solid conducting copper ground. Lastly, the whole structure is supported on a piece of foam.

The parameters and their descriptions, along with their optimised value are presented in Table 5.1 and Figure 5.1.

Table 5.1: Parameters for the Wilkinson Power Divider along with their Optimised Values.

Symbol of Parameters	Description	Optimised Value/ cm
$l_{50 \ 1}$	Length of the first 50Ω line	5.45
$l_{70.71}$	Length of the 70.71Ω line	3.5
$l_{50 \ 2}$	Length of the second 50Ω line	9.56
$l_{50 \ 3}$	Length of the third 50Ω line	14.07
H_{Sub}	Height of the substrate	0.15

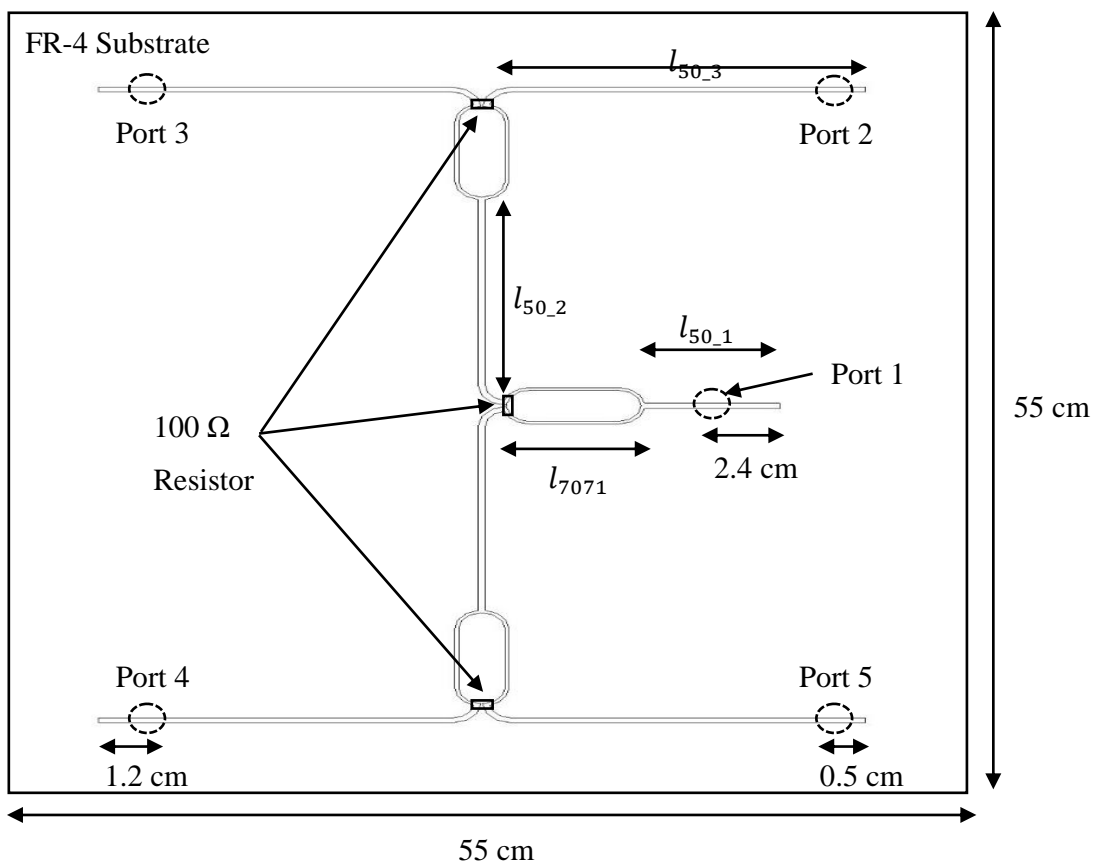
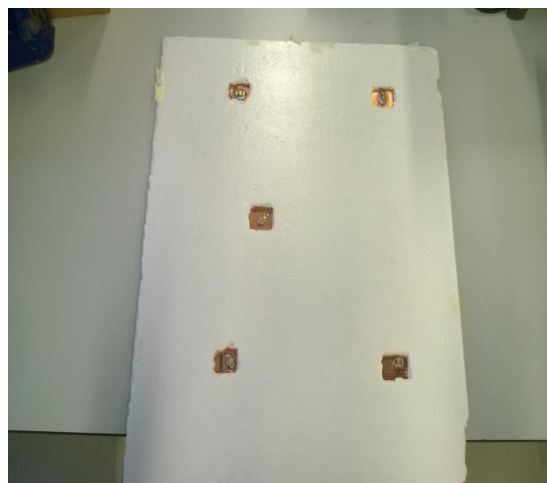


Figure 5.1: Configuration of the Wilkinson Power Divider.



(a)



(b)

Figure 5.2: (a) Top View and (b) Back View of the Fabricated Wilkinson Power Divider.

5.2 Reflection Coefficient

First of all, the reflection coefficient of the power divider is studied. For this case, since there are 5 ports in this power divider, the reflection coefficient refers to the S-parameters of S_{11} , S_{22} , S_{33} , S_{44} and S_{55} , whereby each one represents the reflection coefficient at that particular port.

Figure 5.3 shows the simulated and measured result for the S_{11} parameter. The Wilkinson power divider is designed to work best at 920 MHz, which is within the Malaysia UHF RFID range. From the figure, one can see that the simulated result has a good matching of about -35 dB at 924.5 MHz. Although the frequency is slightly outside the Malaysia UHF RFID range, but due to the high Q-value, the matching from 919 MHz to 923 MHz is still good. As for the measured result, the resonance frequency agrees well with the simulation result, just that the magnitude is much smaller at -17 dB. Since the magnitude is smaller than -10 dB, the measured result is acceptable.

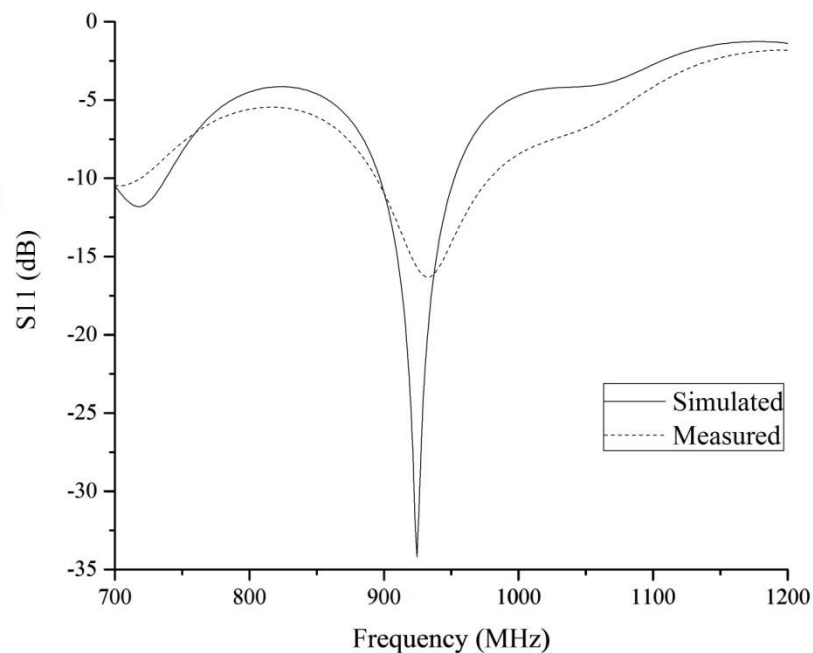
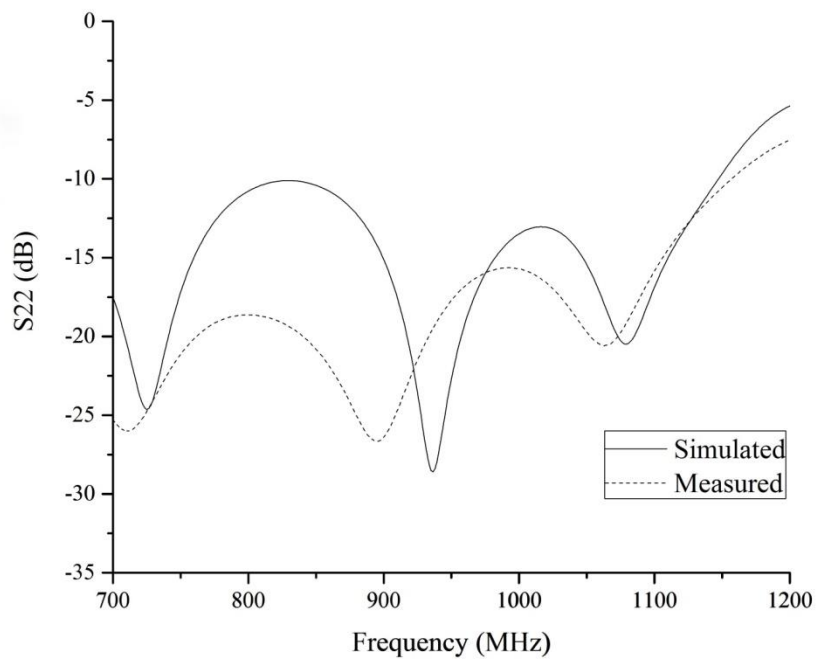


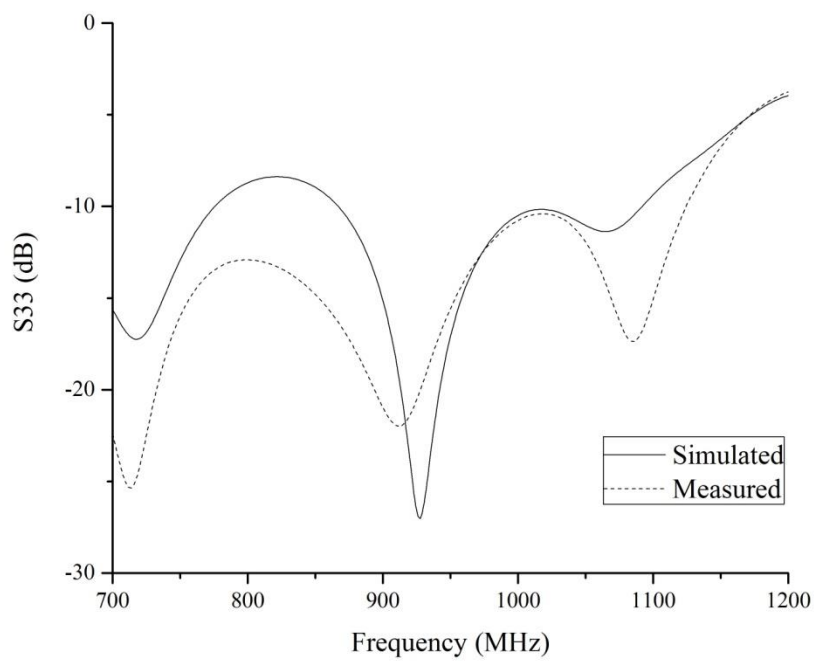
Figure 5.3: Simulated and Measured S_{11} Parameter of the Wilkinson Power Divider.

Figure 5.4(a) to (d) presents the simulated and measured reflection coefficients of port 2, 3, 4 and 5 respectively. In general, the reflection coefficients at the 4 ports have the same trend. For S_{22} , the fabricated prototype is able to achieve a -10 dB impedance bandwidth from 700 MHz to 1145 MHz, which is more than enough to cover the UHF range. The measured resonance frequency has shifted towards 900 MHz. This is slightly lower than the simulated 936 MHz. In terms of magnitude, the measured result shows a better matching whereby the magnitude is smaller than the simulated result at almost all points in the operation bandwidth. For S_{33} , the results are shown in Figure 5.4(b). For port 3, the measured resonant dip occurs at 900 MHz as well. Similar to S_{22} , the measured result is lower than the simulated resonant frequency. Even though the magnitude of the resonant dip at 900 MHz is not as good as the simulated result (-22 dB and -27 dB respectively), the magnitude of the overall reflection loss is better in a sense that the prototype has a larger bandwidth. The measured result shows that the bandwidth of 48.6 % as opposes to the simulated result of 22.4 %. Furthermore, this bandwidth is calculated with the assumption that 700 MHz is the lower limit of the bandwidth. From the trend, one should expect that the bandwidth will be much larger.

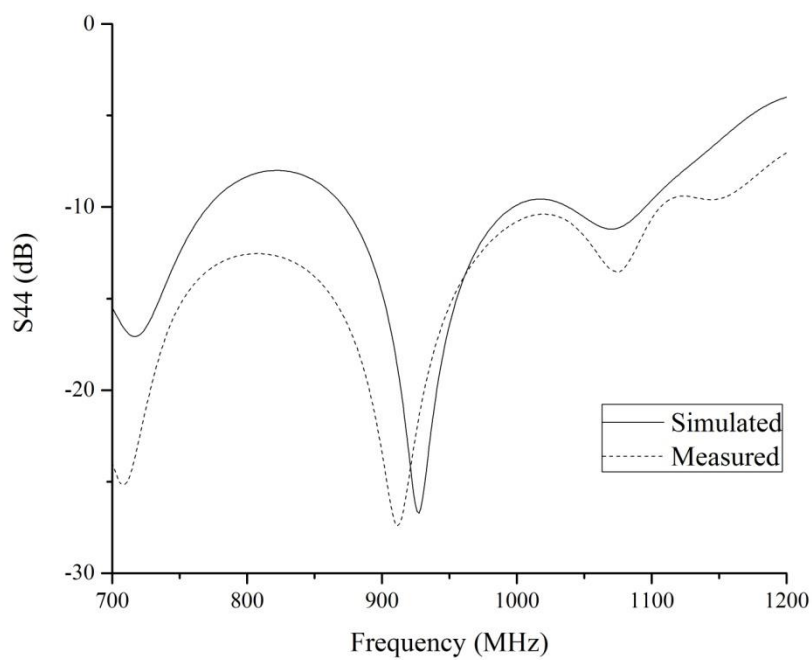
With reference to Figure 5.4(c), the simulated and measured reflection coefficient for port 4 is presented. For this particular port, the measured result agrees well with the simulated one. There is some slight frequency shift of approximately 10 MHz for the resonant dip. Similar to S_{33} discussed above, the impedance bandwidth of the measured result is better than that of the simulated one. The fabricated prototype has an S_{44} parameter of less than -10 dB at almost the whole frequency range of 700 MHz to 1200 MHz, whereas the simulated result only shows a bandwidth from 870 MHz to 990 MHz. Lastly for S_{55} , the result is shown in Figure 5.4(d). The comparison between the simulated and measured is very similar to that of S_{22} , whereby the resonant dip occurs at 900 MHz with a magnitude of -27 dB and the bandwidth is much larger than the simulated bandwidth. One possible reason for the similarity between S_{22} with S_{55} and S_{33} with S_{44} is that both port 2 and 5 is on the right side while port 3 and port 4 are on the left side of the power divider. Since the power divider is symmetrical about the centre 50 Ω strip line, the result measured at the top part should be the same as the bottom result.



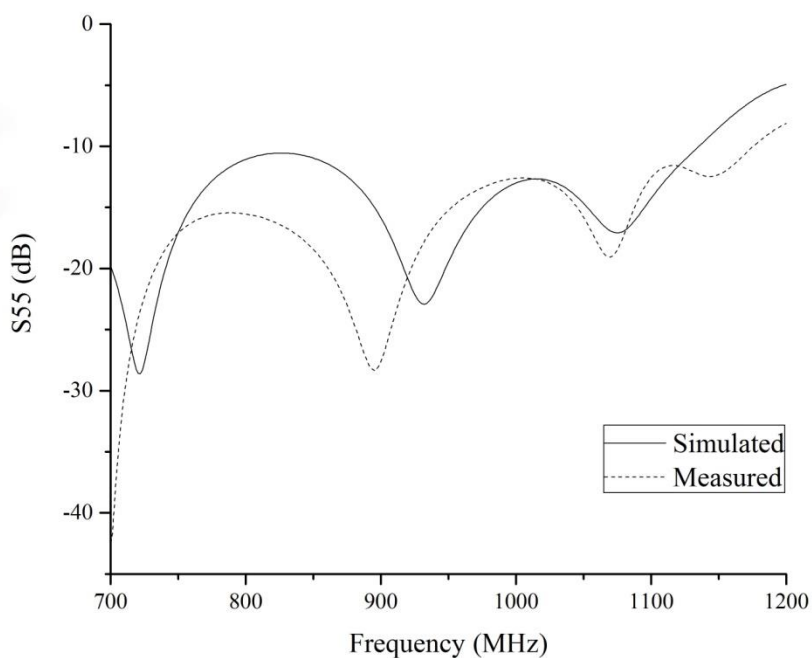
(a)



(b)



(c)



(d)

Figure 5.4: Simulated and Measured Results for (a) S_{22} , (b) S_{33} , (c) S_{44} and (d) S_{55} for the Wilkinson Power Divider.

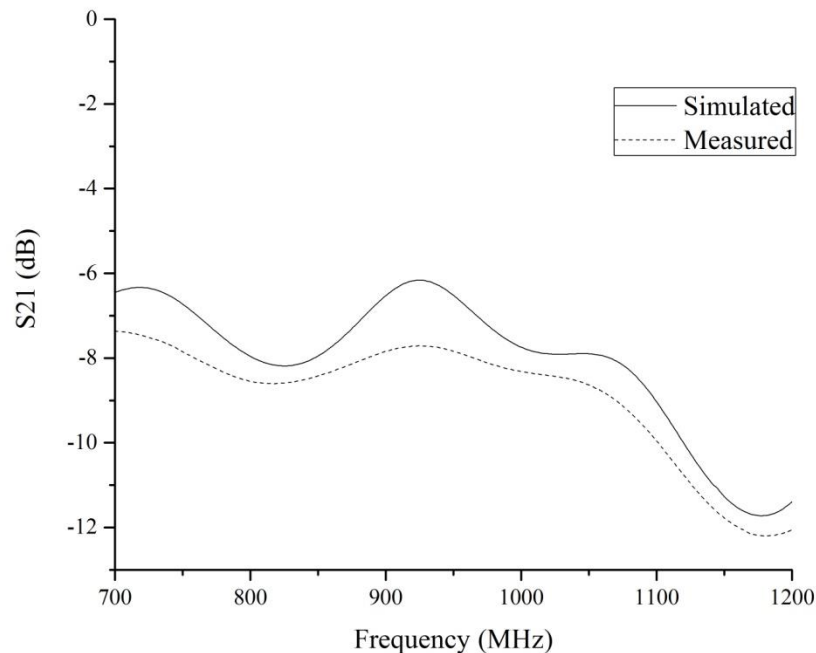
5.3 Insertion Loss

Insertion loss is basically the ratio of the received power at one port relative to the input power at another port. In the case of this Wilkinson power divider, the insertion loss is referring to 4 of the S-parameters: S_{21} , S_{31} , S_{41} and S_{51} . Taking S_{21} as an example, S_{21} measures how much power is loss at port 2 relative to the input power at port 1. Since this design of power divider has an equal power splitting, the value of S_{21} to S_{51} theoretically would equal to -6 dB. This is because -3 dB is equivalent to reducing the power by half, so a -6 dB magnitude would mean the received power is 1/4 of the input power, as expected from a 1-to-4 Wilkinson power divider.

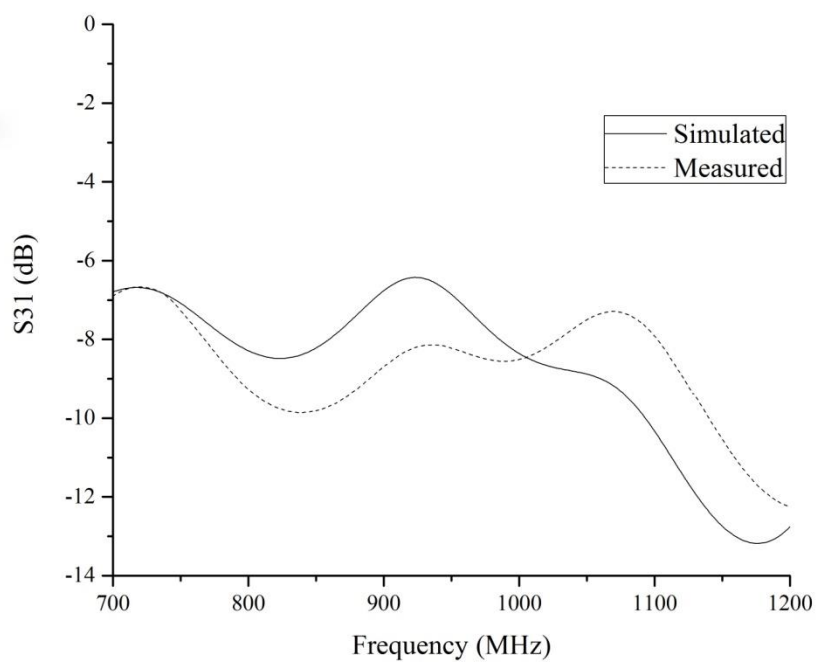
Figure 5.5(a) to (d) show the simulated and measured results for the insertion loss for port 2 to port 5 respectively. The simulated results are first discussed. At around the designed frequency of 920 MHz, one can see that the magnitude of the insertion loss for all 5 ports is at -6 dB, just as the theory has predicted. Since this design of Wilkinson power divider is a simple one, it does not has a wideband operation, so in the UHF range the insertion loss varies from -6 dB to -8 dB. As for the measured result, in general, the results show a similar trend with the simulated one, and thus the discussion will be focused on the magnitude of the insertion loss in the UHF range. For S_{21} shown in Figure 5.5(a), the difference in the magnitude is at around 1 dB in the lower region from 860 MHz to 900 MHz, and it peaks at 920 MHz with a difference of 2 dB. This means that port 2 of the fabricated prototype has only received 16.8 % of the input power at 920 MHz since the magnitude of S_{21} is at -8 dB. A similar trend is seen in S_{31} in Figure 5.5(b). The magnitude of S_{31} varies from the lowest of -10 dB at around 850 MHz to highest of -8 dB at 920 MHz, and the difference is now a constant of 2 dB across the band. There are two main reasons associated with this extra loss in the power received at these two ports. The first reason is due to the intrinsic loss of the FR-4 substrate. During the simulation, a lossless FR-4 is used to simulate the power divider, however, in reality, a perfect lossless substrate is not possible. So this intrinsic loss will cause some of the input power from port 1 to be loss and hence the smaller insertion loss magnitude. The second reason is the gap between the two pieces. Referring to Figure 5.2(a), port 1, 4 and 5 are fabricated on the same piece of FR-4 while port 2 and 3 is printed on

another board. The existence of an air gap, albeit small, is found to cause a significant loss in the power received at the ports. This is clear when the results for port 4 and 5 are discussed. Hence, these two reasons caused the 2 dB difference between the simulated and measured results.

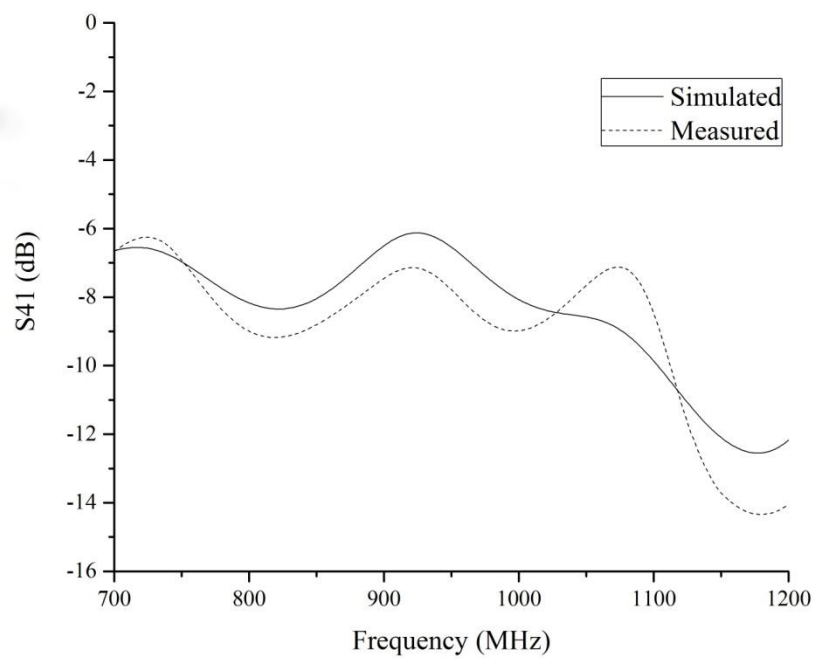
For S_{41} and S_{51} , the results are shown in Figure 5.5(c) and (d) respectively. This two insertion losses are found to have the same characteristics. Both vary from -9 dB to -7 dB in the UHF range and the difference between the simulated and measured result is at a constant of 1 dB. At around 920 MHz, both ports have a magnitude of -7 dB, so this means that the power received from port one is at 20 %. This result supports the fact that the air gap causes extra loss to the power received. Since port 4 and 5 is printed on the same piece as port 1, the only reason for the extra 1 dB loss is due to the intrinsic loss of the FR-4 board. This further suggests that the air gap and patching also causes an extra of 1 dB loss to the power received.



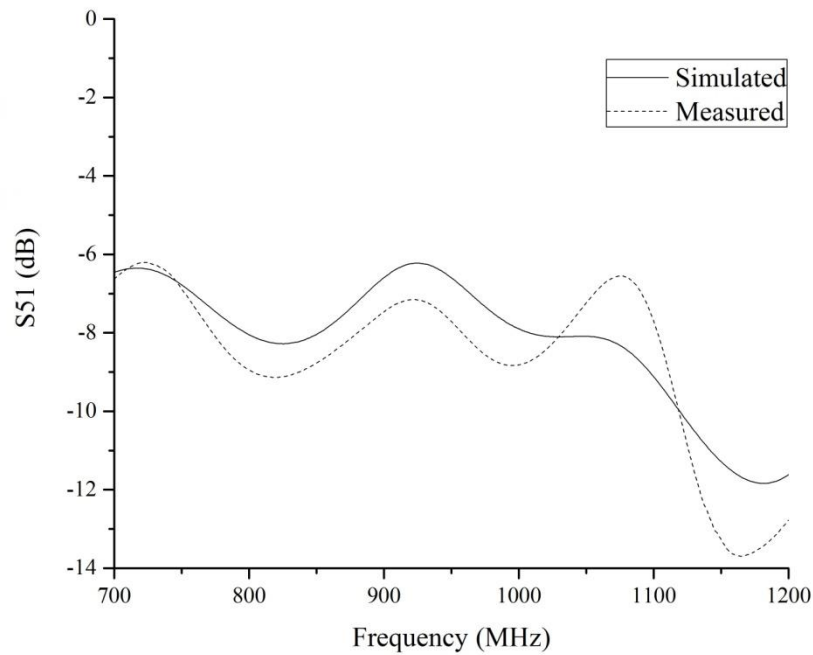
(a)



(b)



(c)



(d)

Figure 5.5: Simulated and Measured Result for (a) S_{21} , (b) S_{31} , (c) S_{41} and (d) S_{51} of the Wilkinson Power Divider.

In conclusion, the fabricated Wilkinson power divider prototype is found to be less efficient than a theoretical one due to the extra losses. Besides that, the power divider is not exactly an equal power splitter since the bottom ports receive more power than the top ports. This is due to the limitation of the etching equipment being not able to etch the whole design in one single piece. If there is such equipment available, the result of the power divider can be made better.

CHAPTER 6

A WIDEBAND CIRCULARLY POLARISED 2×2 ARRAY USING MODIFIED L-SHAPED PROBE

6.1 Array Configuration

The 2×2 array is the combination of the single-element patch antenna discussed in Chapter 4 and the Wilkinson power divider discussed in Chapter 5. First of all, the ports on the Wilkinson power divider are removed and the holes are covered up with solder. Then, 4 identical modified L-shaped probes as shown in Chapter 4 and they are soldered onto the exact location of port 2 to 5. Port 1 is left untouched and it will serve as the input port for the array. As for the radiating patches, the length of the patch is changed to 10.8 cm to optimise the performance of the array. Similar to the single-element antenna, the patches are supported by the means of foam. The horizontal separation of the patches is 18 cm while the vertical separation of the patches is 20.6 cm. Lastly, the whole fabricated prototype is secured on a piece of wood so that the whole array won't wobble during any measurements. The design of the array is shown in Figure 6.1 and Figure 6.2(a) and (b).

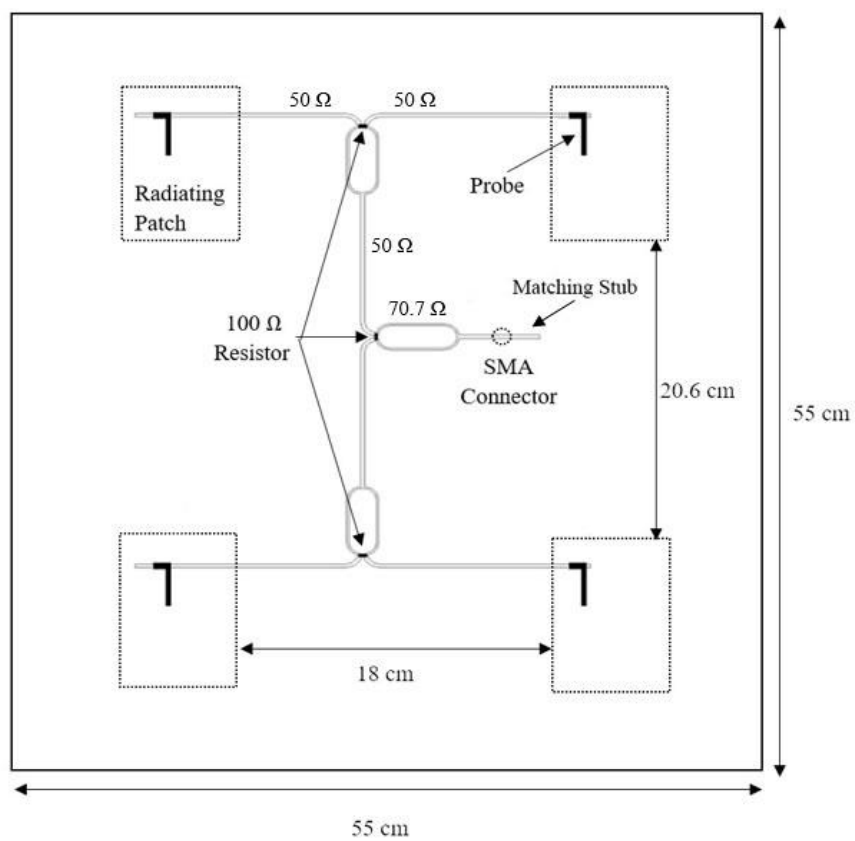
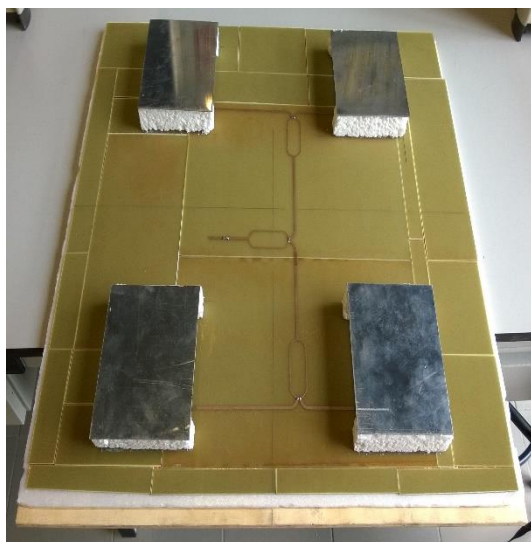
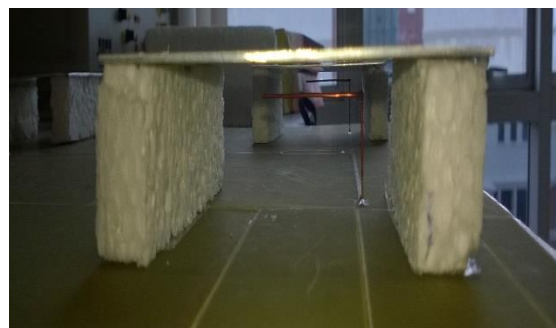


Figure 6.1: Configuration of the 2×2 Array.



(a)



(b)

Figure 6.2: (a) Top View and (b) Side View of the Fabricated Array.

6.2 Reflection Coefficient

Figure 6.3 shows the simulated and measured reflection coefficient of the 2×2 array. There is some slight discrepancy between the simulated and the measured result in terms of resonance frequency and bandwidth. From the figure, the prototype resonates at 960 MHz with a magnitude of -21 dB, as oppose to the simulated frequency of 917 MHz. However, in terms of the impedance bandwidth, the array does have the required 100 MHz bandwidth, but the frequency ranges from 900 MHz to 1000 MHz. This bandwidth is not able to cover the whole UHF range, so further works can be done to bring the bandwidth to start from 860 MHz for universal UHF RFID usage.

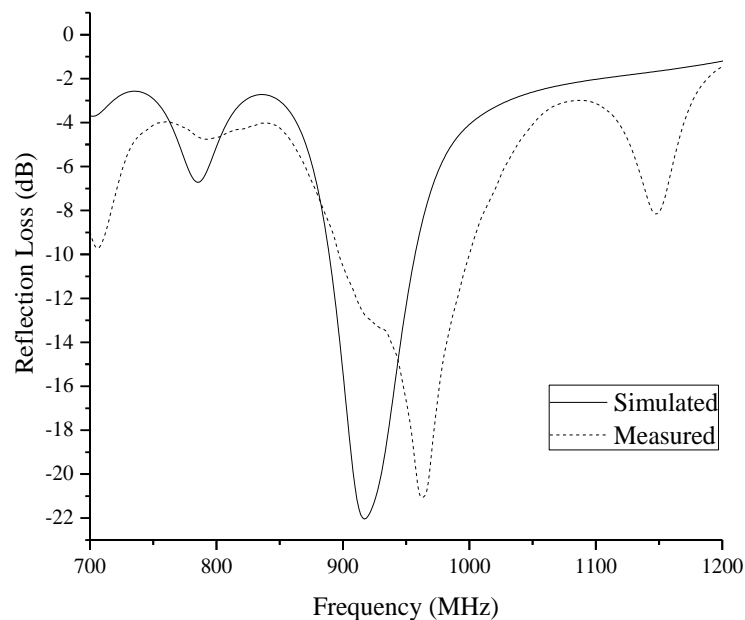


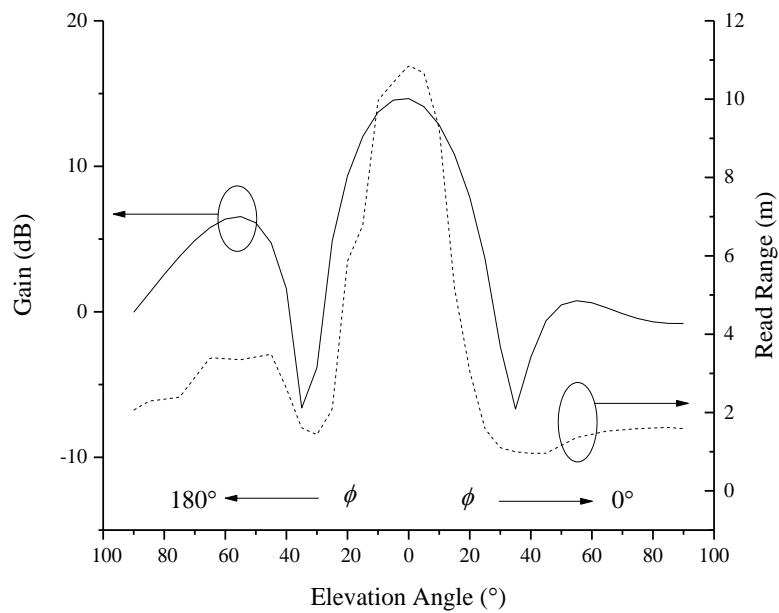
Figure 6.3: Simulated and Measured Reflection Coefficient of the Array.

6.3 Radiation Patterns and Read Range

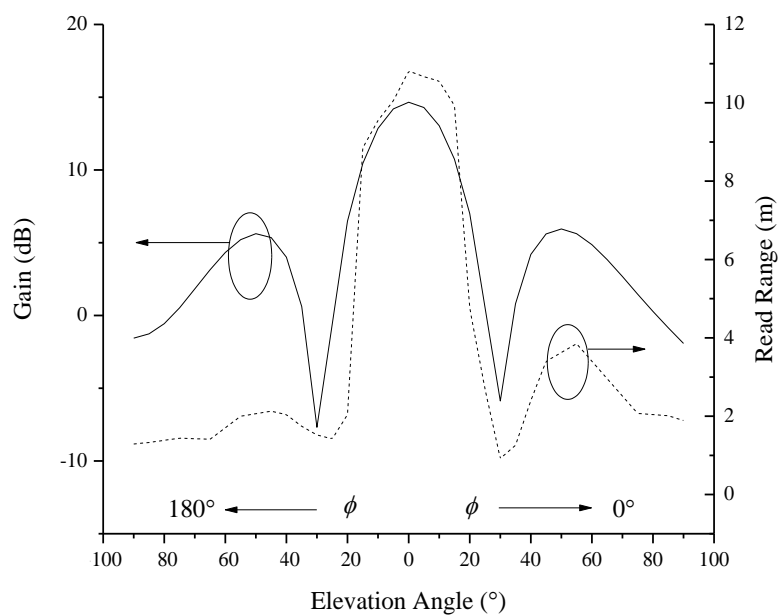
Similar to the single-element antenna, the radiation patterns are measured in terms of the read range from 90° ($\phi \rightarrow 0^\circ$) to 90° ($\phi \rightarrow 180^\circ$), using the same technique described in Chapter 4. The simulated gain and the measured read range in the x - z plane at 920 MHz are shown in Figure 6.4(a). Due to the array configuration, the radiation pattern is more complicated than the single-element antenna. For the array, the peak gain occurs at 0° with a magnitude of 14.7 dB and there exists a secondary maxima at 55° . The pattern is not symmetrical about the centre such that the secondary maximum peak at 55° ($\phi \rightarrow 180^\circ$) is larger than the one at 55° ($\phi \rightarrow 0^\circ$). The magnitudes are 6.51 dB and 0.73 dB respectively. On the other hand, the minimum gain occurs at 35° with a gain of approximately -6.7 dB. The measured read range reflects the trend of the simulated gain. The maximum read range occurs at 0° at 10.9 m and decreases rapidly until the minimum of about 1 m at 35° . After here, there is some difference between the two angular directions. Since the gain at the $\phi \rightarrow 180^\circ$ side is larger than the one of the $\phi \rightarrow 0^\circ$ side, and the read range is also larger as well. This is shown in Figure 6.4(a) where the secondary maximum read range at 55° ($\phi \rightarrow 180^\circ$) is approximately 3 m while at 55° ($\phi \rightarrow 0^\circ$), it is only about 1.5 m.

Next, the pattern in the y - z plane is shown in Figure 6.4(b). As compared to the x - z plane, the radiation pattern in this plane is more symmetrical about 0° . The value of the peak gain and the magnitude is the same as above at 0° with a gain of 14.7 dB. As for the secondary maxima, they occur at 50° with magnitudes of 5.6 dB and 5.9 dB respectively. The minimum now occurs at 30° instead of the 35° in the x - z plane. When it comes to the read range, the measured result does reflect the simulated gain, but only before the angle of 30° . The read range peaks at 0° with the same maximum read range and decreases as the elevation angle increases until 30° . After that, one would expect that the read range is similar in both the direction due to the symmetrical gain pattern. However, the measured result shows that the read range in the $\phi \rightarrow 0^\circ$ side is larger than that of the $\phi \rightarrow 180^\circ$ direction. To illustrate further, the secondary maximum read range peaks at about 4 m on the $\phi \rightarrow 0^\circ$ side

while on the $\phi \rightarrow 180^\circ$ side it is only 2 m. This suggests that the actual gain pattern is not symmetrical but is skewed towards the $\phi \rightarrow 0^\circ$ side.



(a)



(b)

Figure 6.4: Simulated Gain and the Measured Read Range in the (a) x - z plane and (b) y - z plane at 920 MHz.

6.4 Axial Ratio

Figure 6.5 presents the simulated and measured axial ratio of the 2×2 array. From the figure, the proposed array is able to achieve a CP bandwidth of 5.4 % (910 MHz – 960 MHz) with a lowest axial ratio magnitude of 0.4 dB at 940 MHz. When compared to the simulated result, the measured result agrees well in terms of the bandwidth, trend and also the magnitude. However, the operation bandwidth is slightly different where the measured bandwidth is at the higher frequencies. Even though the array is not able to achieve a CP operation in the whole UHF range, it still has the potential to be used as a CP reader antenna in Malaysia and some other countries.

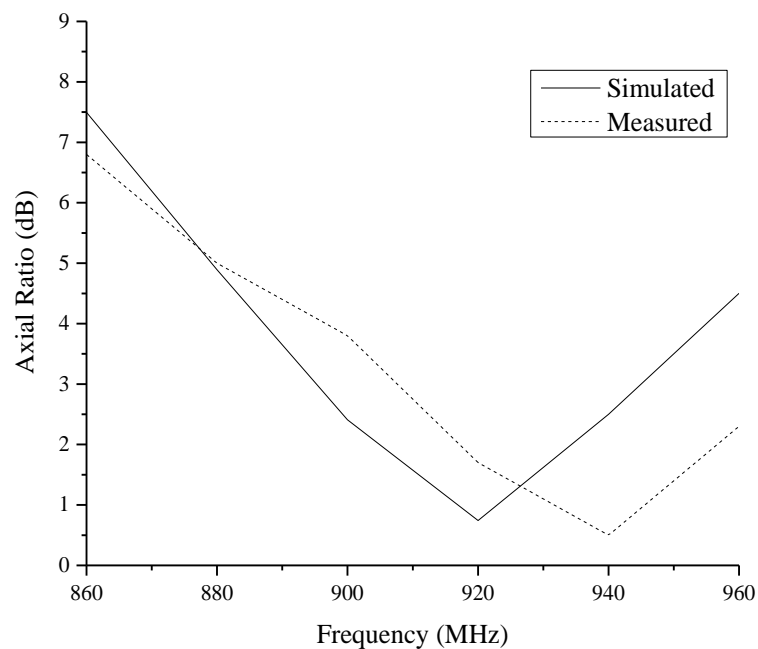


Figure 6.5: Simulated and Measured Axial Ratio of the 2×2 Array.

CHAPTER 7

CONCLUSION AND RECOMMENDATIONS

In this dissertation, a novel modified L-shaped probe which consists of 3 sides is proposed as a mean to excite a patch for the purposes of UHF RFID reader antenna. The whole project consists of three parts: the single element antenna, the Wilkinson power divider, and the 2×2 array. The performance of the design is simulated, and prototypes were built to confirm the simulation models. Good agreement is found between the simulation and the measured results. For the single-element antenna, the impedance bandwidth and the CP bandwidth are found to be from 760 MHz to 990 MHz and 890 MHz to 940 MHz respectively. The maximum read range is 6.3 m. A parametric analysis is done for the single-element antenna as well. For the Wilkinson power divider, it is found that there exists some extra loss due to the air gap and the substrate, so the insertion loss for the four ports varies from -9 dB to -7 dB in the UHF range. Lastly is the 2×2 array, which is basically the combination of the single-element antenna and the Wilkinson power divider. The impedance and CP bandwidth are from 900 MHz to 1000 MHz and 910 MHz to 960 MHz respectively, while the maximum read range is at 10.8 m.

In the future, works can be done to increase the CP bandwidth of the antenna such that it can cover the whole UHF range from 860 MHz to 960 MHz. Besides that, the bandwidth of the array can be shifted slightly to the lower frequencies for universal usage as well. Both antennas have the potential to be used as UHF RFID reader antennas.

REFERENCES

- Bahl, I. and Trivedi, D. (1977). *A Designer's Guide to Microstrip Line*. pp.174 - 182.
- Balanis, C. (2005). *Antenna theory*. Hoboken, NJ: Wiley Interscience.
- Boo, Y., Nasimuddin, Chen, Z. and Alphones, A. (2009). Broadband circularly polarized microstrip antenna for RFID reader applications. *2009 Asia Pacific Microwave Conference*.
- Chen, B. and Sim, C. (2014). Broadband circularly polarized stacked patch antenna for universal UHF RFID applications. *2014 International Symposium on Antennas and Propagation Conference Proceedings*.
- Garg, R. (2001). *Microstrip antenna design handbook*. Boston, MA: Artech House.
- Liu, X., Liu, Y. and Tentzeris, M. (2015). A Novel Circularly Polarized Antenna With Coin-Shaped Patches and a Ring-Shaped Strip for Worldwide UHF RFID Applications. *Antennas Wirel. Propag. Lett.*, 14, pp.707-710.
- Mak, C., Luk, K., Lee, K. and Chow, Y. (2000). Experimental study of a microstrip patch antenna with an L-shaped probe. *IEEE Trans. Antennas Propagat.*, 48(5), pp.777-783.
- Nikitin, P. and Rao, K. (2010). Helical Antenna for Handheld UHF RFID Reader. *IEEE RFID*.
- Pozar, D. (2005). *Microwave engineering*. Hoboken, NJ: J. Wiley.

Sim, C. and Hsu, Y. (2013). Circularly Polarized Equilateral Triangle Patch Antenna for UHF RFID Reader Applications. *Loughborough Antennas & Propagation Conference*.

Sun, J. and Lee, Y. (2008). Circularly polarized stacked antenna with a high-impedance ground plane for RFID reader applications. *Microwave and Optical Technology Letters*, 50(9), pp.2248-2250.

Tang, Z., Zhan, J. and Liu, H. (2012). Dual-resonance compact circularly polarized reader antenna for UHF RFID applications. *Microwave and Optical Technology Letters*, 54(11), pp.2531-2533.

Tiang, J., Islam, M., Misran, N. and Singh, J. (2014). Wideband L-probe circular patch antenna for dual-frequency RFID application. *Microwave and Optical Technology Letters*, 56(6), pp.1421-1424.

Wang, Z., Fang, S., Fu, S. and Jia, S. (2011). Single-Fed Broadband Circularly Polarized Stacked Patch Antenna With Horizontally Meandered Strip for Universal UHF RFID Applications. *IEEE Transactions on Microwave Theory and Techniques*, 59(4), pp.1066-1073.

Wang, Z., Fang, S., Fu, S. and Mujie Fan, (2010). Single-fed single-patch broadband circularly polarized antenna for UHF RFID reader applications. *2010 2nd International Conference on Industrial and Information Systems*.

Xu, J., Chen, Z. and Qing, X. (2012). A Broadband Circularly Polarized Antenna. *IEEE Asia-Pacific Conference on Antennas and Propagation*.

Yeh, C., Chen, B., Chen, C. and Sim, C. (2015). L-shaped probe feed patch antenna with circular polarization radiation for UHF RFID applications. *2015 IEEE MTT-S 2015 International Microwave Workshop Series on RF and Wireless Technologies for Biomedical and Healthcare Applications (IMWS-BIO)*.